NASA TECHNICAL NOTE

A FLIGHT INVESTIGATION OF ABLATION ON A BLUNTED CYLINDER-FLARE CONFIGURATION TO A MACH NUMBER OF 8.48

by Clyde W. Winters and William G. Witte

Langley Research Center
Langley Station, Hampton, Va.

A FLIGHT INVESTIGATION OF ABLATION ON A

BLUNTED CYLINDER-FLARE CONFIGURATION

TO A MACH NUMBER OF 8.48

By Clyde W. Winters and William G. Witte

Langley Research Center
Langley Station, Hampton, Va.

NATIONAL AERONAUTICS AND SPACE ADMINISTRATION

A FLIGHT INVESTIGATION OF ABLATION ON A

BLUNTED CYLINDER-FLARE CONFIGURATION

TO A MACH NUMBER OF 8.48

By Clyde W. Winters and William G. Witte
Langley Research Center

SUMMARY

A three-stage rocket-propelled research-vehicle system was flown to a maximum Mach number of 8.48 at an altitude of 25,000 feet, to determine the ablation characteristics of Teflon in free flight. Continuous in-flight measurements were made on the front face of the model by using variable-capacitance sensors. The ablated-length measurements were in good agreement with analytical predictions. In addition, temperature measurements were obtained under an unprotected inconel segment and a Teflon and inconel composite segment on a cylindrical test section and on the stabilizing flare of the model. Heating rates computed from these measurements were in good agreement with predicted values. An NASA computer program was used to obtain temperature histories and ablation rates on the Teflon and inconel composite cylindrical test section. Inside inconel wall temperatures obtained from this program were in good agreement with measured temperatures.

INTRODUCTION

Within the past decade ablation materials have become of particular interest to the aerodynamicist. The use of ablators for thermal protection on high-speed bodies has become an accepted compromise between weight and protective temperature.

The early work in this field had as a prime objective the qualitative assessment of the potentials of ablating materials as related to heating rates encountered during flight. A theoretical treatment (ref. 1), for ablating materials which sublime rather than melt, has indicated certain desirable properties for such materials. Other studies have shown that the absorption of heat involves a number of complex mechanisms which require knowledge of the material properties in various states for a complete analytical treatment.

As work progressed in this field, it became apparent that the heat-blocking capacity or potential of ablating materials depended very strongly on the enthalpy difference across the boundary layer (ref. 2). Experiments were

conducted at both low and high enthalpies and the results clearly indicated
that the enthalpy parameter has a powerful effect. Ensuing experimental and
analytical work (ref. 3) produced procedures suitable for predicting the effec-
tive heats of ablation.

In view of NASA objectives to fly supercircular-velocity spacecraft with
eventual reentry in the earth's atmosphere, the Langley Research Center under-
took a flight-test research project to verify these ablation parameters under
actual flight conditions (ref. 4). The data thus obtained would provide a
basis for the design information needed for the missions with high velocity
requirements.

This report describes the performance of the ablation material, Teflon,
for a particular flight trajectory. Teflon was chosen for the test material
because its physical and thermal properties were relatively well known and a
working Teflon ablation sensor had been developed (ref. 5). The flight test
was made by use of a three-stage solid-propellant rocket which carried the test
model to a maximum Mach number of 8.48 at an altitude of 25,000 feet. Ablated-
length measurements were made over a Mach number range increasing from 5.30
to 8.48 and then decreasing to 5.85. The corresponding free-stream Reynolds
number ranged from 22×10^6 to 28×10^6 and then decreased to 4.3×10^6.

Besides the ablation data on the nose, temperature measurements were made
so that the heat transfer on the model cylindrical section and the stabilizing
flare could be determined.

SYMBOLS

c_p specific heat at constant pressure, Btu/lb-$^\circ$R

g acceleration due to gravity, 32.2 ft/sec^2

h_{eff} effective heat of ablation, Btu/lb

H enthalpy, Btu/lb

J mechanical equivalent of heat, 778.26 ft-lb/Btu

l length, in.

M Mach number

$\dot{m}$ ablation rate, lb/(sq ft)(sec)

q heating rate, Btu/(sq ft)(sec)

R Reynolds number per foot

r lateral radius of nose, in.

r_c	radius of curvature of nose, in.
ρ	density, lb/cu ft
ρ_c	density of Teflon vapor, lb/cu ft
s	distance along the model surface, measured from the stagnation point, in.
T	temperature, $^{\circ}R$ or $^{\circ}F$ as indicated
t	time, sec
V	velocity, ft/sec

Subscripts:

aw	adiabatic wall
c	coolant or Teflon gas
l	local
sl	sea level
o	initial condition
t	stagnation
w	wall outer surface
∞	free stream

MODEL DESCRIPTION

The final stage of a three-stage rocket was used for the test model. (See fig. 1.) Three sections of this model, the nose cone, the cylinder, and the stabilizing flare (fig. 2), were specially constructed and instrumented for the testing and analysis of Teflon. The primary objective of the test was to measure Teflon ablation on the nose of the model. In order to minimize the variables of this test a nose shape was chosen that had essentially constant heating rates across its surface. Secondary objectives of the test were to measure the effectiveness of Teflon coatings on the cylinder and flare of the model.

Nose Cone

The Teflon nose cone (fig. 3) was a body of revolution 12.10 inches in length, having a blunted face with $r/r_c = 1/3$ and a 10° half-angle flared

3

afterbody. Five ablation sensors were mounted as shown in figure 3. The longitudinal axes of the sensors were normal to the surface and in a plane passing through the axis of revolution of the Teflon nose. Sensor 2 was located on the front face at the stagnation point. Sensors 1 and 3 were located on the front face, also, at s/r = 0.62. Sensors 4 and 5 were located on the 10° flare. Ablation data are presented only for sensors 2 and 3. Sensors 1, 4, and 5 became defective prior to the test portion of the flight.

Cylindrical Test Section

The cylindrical test section consisted of the forward 12 inches of the cylindrical portion of the model. Figures 2 and 4 show the geometry and instrumentation of this section. The test section was divided axially into two equal segments. One segment was made of 0.077-inch inconel. The other segment was a composite of 0.032-inch Teflon sheet bonded to 0.052-inch inconel, with the external layer being Teflon. Three 30-gage chromel-alumel thermocouples were spotwelded to the inside inconel wall of each segment at the locations indicated in figures 2 and 4. Temperature measurements were obtained for all six locations.

Stabilizing Flare

The 10° half-angle stabilizing flare of the third-stage sustainer motor (fig. 2) was treated in a manner similar to the cylindrical test section described previously. It was divided axially into two equal segments, with one segment made of 0.077-inch inconel and the other a composite of 0.032-inch Teflon sheet bonded to 0.055-inch inconel, with the external layer being Teflon. Two 30-gage chromel-alumel thermocouples were spotwelded to the inside inconel wall of each segment at the locations shown in figure 2. Temperatures were obtained under the unprotected inconel segment, but both thermocouples under the composite malfunctioned and no data were obtained for that segment.

INSTRUMENTATION AND TELEMETRY

The instrumentation for the flight consisted of 4 linear accelerometers, 5 Teflon ablation sensors, and 10 thermocouples. A standard 10-channel telemeter was used to transmit the data from the model to the ground station. The linear accelerometers, the thermocouple commutator, and the telemeter package were located in the cylindrical test section forward of the third-stage sustainer motor.

Four channels of the 10-channel telemeter were used for the 4 linear accelerometers. Two accelerometers measured longitudinal accelerations, one measured normal accelerations, and one measured transverse accelerations.

A single commutated channel was used for telemetering the thermocouple data. It was commutated so that five temperature readings per second were obtained for each of the 10 thermocouples.

Five channels were used for the five Teflon ablation sensors. The Teflon ablation sensor is a device that is used to obtain in-flight measurements of changes in the thickness of Teflon as a result of ablation. The data from the sensor are transmitted through the telemeter as oscillator frequency changes. A description of this sensor is presented in appendix A.

LAUNCH VEHICLE AND FLIGHT TRAJECTORY

The assembled vehicle is shown in figure 5. The flight trajectory from the launch vehicle was such as to produce an appropriate environment for the evaluation of the Teflon ablation material. The propulsion system consisted of three stages which were solid-propellant rocket motors. The first and second stages were fin-stabilized Nike M5 rocket motors. The third-stage sustainer was a flare-stabilized XM19 Recruit rocket motor. A cylindrical transition section formed a permanent attachment between the third-stage sustainer motor and the Teflon nose.

The vehicle was ground launched at an elevation angle of 68° from the horizontal on an azimuth of 80° from true north. The measured flight trajectory, altitude plotted against range, is shown in figure 6. Notations are made on the figure to indicate the time sequence of various events.

Time histories of the velocity and altitude are shown in figure 7. The curves were obtained from radar data. As a check on the velocity obtained from the radar, the histories of the longitudinal accelerometers were integrated and the values obtained are shown by circular symbols. The accelerometer data essentially follow the data obtained from the radar; however, the accelerometer data were used in reducing the data from the model. Two hours before launch, the density, temperature, and wind variation were measured to an altitude of 91,000 feet. The variation of the ambient values of density and temperature with time are shown in figure 8, along with the calculated variation of the flight stagnation temperature. The time histories of free-stream Mach number and free-stream Reynolds number per foot are shown in figure 9.

The test environment ranged from an altitude of 18,000 feet to 63,000 feet, over a Mach number range increasing from 5.85 to 8.48 and then decreasing to 5.80 with corresponding free-stream Reynolds numbers per foot increasing from 22.0×10^6 to 28.0×10^6 and then decreasing to 4.30×10^6. The environmental conditions presented in this section were used in the reduction of the data obtained from this experiment.

RESULTS AND DISCUSSION

The ablation measurements on the Teflon nose and the temperature measurements and heating rates on the cylindrical test section and on the stabilizing flare are presented in this section. Also presented here are the results of two methods of predicting the ablation characteristics of Teflon. One method

predicts the ablated-length changes of the Teflon nose. The other method predicts ablation rates and temperature histories on the cylindrical test section. The results and discussions are presented in three sections, one for each of the three model test sections.

Teflon Nose

The ablation data obtained during the flight between $M = 5.30$ and $M = 8.48$ from sensors 2 and 3 are presented in figure 10 as ablated length plotted against time; these measured values are indicated by circular and square symbols, respectively. Values are shown from $t = 7.0$ seconds to $t = 15.5$ seconds. Prior to $t = 7.0$ seconds and after $t = 15.5$ seconds the sensors indicated no measurable ablation.

In figure 11, the effective heat of ablation h_{eff} is shown as a function of the modified enthalpy potential parameter $\left(H_{aw} - H_w\right)\frac{c_{p,c}}{c_{p,l}}\left(\frac{T_l}{T_w}\right)^{0.19}$. These data were obtained in the modified enthalpy potential range for Teflon of 150 to 1,150 Btu/lb. Theoretical effective heats of ablation and heating rates for the nose sensors during the test are presented in figure 12. These data of figures 11 and 12, used in conjunction with other information obtained from reference 3, permit ablated-length changes to be computed. Basically, the computation method involves the use of empirical relationships which define the behavior of ablative materials in general and of Teflon in particular. It is of interest to compare the results determined by calculation with those measured during flight. Therefore, computations were made which corresponded to the flight time from 7.0 seconds to 15.5 seconds. These data are shown by the solid curves of figure 10. The mechanics of the computational procedure are tedious and appendix B has been included to describe the method used and the derivations of the curves presented in figures 11 and 12.

The agreement between the computed ablated-length changes and the measured data of figure 10 is excellent. With the exception of a few data points the experimental data agree with that predicted by theory. The ablated-length changes with time are essentially the same for both sensors on the front face. The sensor located at the stagnation point (sensor 2) indicated an ablated length of 0.072 inch, whereas the sensor located at $s/r = 0.62$ (sensor 3) indicated an ablated length of 0.077 inch.

The solid curve shown in figure 13 was obtained from figure 7 of reference 3 and is the predicted effectiveness of Teflon for the three-dimensional laminar stagnation-point case. The measured ablation data from the front-face sensors are indicated by data symbols. This figure illustrates again the good agreement between the flight data and theory.

6

Cylindrical Test Section

Cylinder heat transfer.- Faired curves showing the variation of inside wall temperature with time for the segment of unprotected 0.077-inch inconel and the composite segment of 0.052-inch inconel and 0.032-inch Teflon are plotted in figure 14. The temperatures for the thermocouples in the same rearward location, but in diametrically opposed positions are shown together. The temperature histories demonstrate clearly the thermal protection provided by an ablation coating. The temperature rise of the thinner inconel sheet covered with Teflon is less than half that of the thicker unprotected inconel sheet.

Experimental heating rates for the 0.077-inch inconel segment are indicated in figure 15 by circular symbols. The computational method of reference 6 was used to obtain these values. In this method, a thermally thick wall with no heat flow parallel to the plate and no plate curvature is considered. The data of figure 14 were used to compute the outside surface temperatures and then the outside surface temperatures were used to compute the one-dimensional heating rate presented in figure 15.

The measured flight aerodynamic conditions were used in conjunction with laminar and turbulent heat-transfer theories to obtain theoretical heating rates for the cylindrical test section. These data are shown in figure 15. The theoretical heating rates for a turbulent boundary layer were computed by the method of reference 7.

The agreement between the experimental data and the turbulent theory is very good up to t = 10.0 seconds, after which the experimental rates approach and intercept the laminar-theory curve. The lowered heating rates may indicate downstream cooling effects due to the ejection of coolant mass from the Teflon nose into the boundary layer. However, computations of downstream cooling effects were inconclusive, because of the uncertainty of flow conditions and ablation rates along the cone flare of the Teflon nose.

Cylinder ablation.- The in-flight ablation performance of relatively thin Teflon sheets, such as the layer in the composite segment of the cylindrical test section, cannot be measured directly at present by ablation sensors or other means. However, a good accounting of the performance may be obtained with the assistance of a Langley Research Center computer program based on the analysis of reference 8. Material properties and trajectory parameters are the primary inputs for the program. Among the outputs received from the program are surface temperatures, inside wall temperatures, and ablation rates. It should be noted that when a constant value for ablation temperature is assumed, the program shows no ablation until the surface temperature reaches this value, and then during ablation the surface temperature is limited to this assumed value. The computer program was used to obtain the temperatures and the ablation rates plotted in figure 16. As shown by the flattened portion of the Teflon surface-temperature curve during the time of ablation, an ablation temperature of 1,200° F was assumed. The deflection in the surface-temperature curve, starting at about 6.5 seconds, is a result of the change in enthalpy due to the decrease in free-stream velocity after burnout of the second-stage motor. Also plotted in figure 16 and indicated by circular symbols are the measured

7

inside wall temperatures along the composite segment. Although several sources have listed different values for thermal conductivity of Teflon, the value used in this study is 35.5 Btu/(sq ft)(sec)(^{O}F/ft). When this value was used in the computer program, good agreement between the measured and the computed inside wall temperatures was obtained as shown in figure 16. This agreement increases confidence in the reliability of this value.

A comparison of the curves for the three thermocouple locations shows that the ablation rates are essentially constant. This result is expected because the heating rates for the three locations were essentially constant also.

Stabilizing Flare

Flare heat transfer.- Faired temperature histories of the inside wall temperatures measured under the inconel segment of the stabilizing flare are shown in figure 17. The temperatures are consistent with each other as well as with temperatures measured on other parts of the model.

Experimental heating rates based on the measured temperatures were computed by the method of reference 6. These values are indicated by circular symbols in figure 18. Theoretical turbulent heating rates were computed by the method of reference 7, and are indicated by the solid lines in figure 18. The experimental heating rates and the theoretical turbulent heating rates are in close agreement.

CONCLUDING REMARKS

A free-flight investigation was made of the ablation rates and shielding effects of Teflon in high-speed flight through the atmosphere. Ablated-length measurements were made on the front face of the test model and temperature measurements were made on a cylindrical test section and on the stabilizing flare.

The ablation data obtained on the front face of the Teflon nose were in excellent agreement with theory. Ablated-length time histories computed from theoretical Teflon ablation relationships matched very closely the measurements obtained from ablation sensors. Also, the measured effectiveness of the Teflon agreed closely with predicted effectiveness.

Measured heating rates for the cylindrical test section were in good agreement with theoretical turbulent heating rates for more than half of the test portion of the flight. But during the last part of the test, the measured heating rates diminished below the theoretical turbulent values and finally diminished below theoretical laminar values.

A Langley Research Center computer program was used to obtain an analysis of the ablation rates and temperature distributions of the composite Teflon and inconel segment located in the cylindrical test section. The inside wall temperatures obtained from the program were in good agreement with the measured inside wall temperatures. This agreement indicates that the computer program

can give an accurate accounting of the performance of an ablating material such as Teflon and, therefore, can be used in the design of an ablation coating.

The measured heating rates on the stabilizing flare were in good agreement with theoretical turbulent heating rates.

Langley Research Center,
    National Aeronautics and Space Administration,
   Langley Station, Hampton, Va., March 25, 1964.

SENSOR TELEMETERING SYSTEM AND CALIBRATION PROCEDURE

Sensor Telemetering System

Inasmuch as the ablation sensor is a capacitor, it can easily be used in a telemetering system using an inductance-capacitance oscillator. The standard NASA subcarrier oscillator channels in the range of 100,000 to 200,000 cycles per second are ideally suited for telemetering the small capacitance changes involved. By connecting the capacitor across the parallel-inductance and capacitance circuit of the oscillator, a change in capacitance will be indicated by a change in frequency of the oscillator. The main frequency-determining element of an inductance-capacitance oscillator is the resonant parallel-inductance—capacitance circuit.

The variable-capacitance ablation sensor is connected in parallel with the main capacitance of the inductance-capacitance oscillator circuit that determines the subcarrier frequency. The hookup of an ablation sensor in an inductance oscillator circuit is shown in the following schematic:
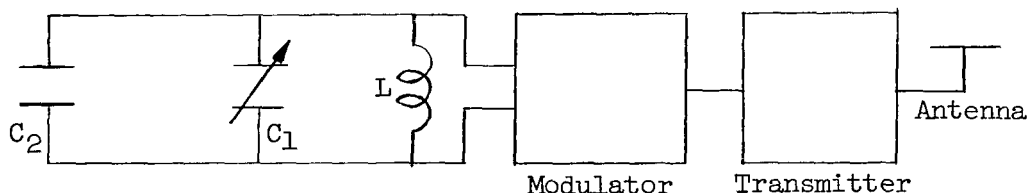
where

C_1 variable capacitor to adjust oscillator, tuning capacitance when used elsewhere

C_2 ·   variable-capacitor ablation sensor, sensor capacitance when used elsewhere

L   tuning coil with five taps, inductance of coil when used elsewhere

As the ablation proceeds, the capacitance of the sensor decreases and the subcarrier frequency of the oscillator f correspondingly increases. The associated vacuum-tube circuitry has a negligible effect on the frequency so that the initial frequency is determined by the usual equation

$$f = \frac{1}{2\pi\sqrt{L(C_1 + C_2)}} \qquad (A1)$$

The variation of the frequency Δf with variation of sensor capacitance ΔC_2 is given by the equation

$$\frac{\Delta f}{f} = -\frac{1}{2}\frac{\Delta C_2}{C_1 + C_2} \tag{A2}$$

For linearity, it is desirable that C_1 be large relative to C_2 in order that the fractional variation of the total capacitance $C_1 + C_2$ be relatively small.

As an example, take the capacitance C_2 of a 0.75-inch-long sensor to be 250 micromicrofarads. Then, with $L = 0.7$ millihenry (the first of the five taps of the inductance coil of the standard NASA subcarrier oscillator) and with C_1 adjusted so that $C_1 + C_2 = 3,245$ micromicrofarads, the frequency is 108,500 cycles per second. Consider that 0.5-inch length decrease of the ablation sensor will decrease the capacitance by 166 micromicrofarads and the frequency will increase by 2,780 cycles per second, which is approximately the desired value of Δf for proper sensitivity. Using the next tap on the coil would have given a value of Δf slightly above 3,000 cycles per second, which is also acceptable.

Calibration Procedure

The ablation sensors cannot indicate length changes directly; however, as the length changes, the frequency shifts on the telemeter record. The frequency shifts can then be converted to length changes by means of a calibration curve of length as a function of frequency.

Since no calibration of capacitance as a function of length is possible without consuming the sensor, the direct proportionality of capacitance to length as indicated in figure 19 was assumed. This assumption, with a calibration of the oscillator frequency as a function of sensor capacitance, provided the curve of frequency as a function of sensor lengths shown in figure 20; this curve was used to interpret the test results.

APPENDIX B

AN ANALYTICAL METHOD FOR DETERMINING ABLATED-LENGTH CHANGES

Computation Procedure

The ablated-length curves of figure 10 may be computed from

$$l - l_o = \frac{1}{\rho_c} \int \dot{m} \ dt \tag{B1}$$

which is a rearrangement of the basic ablation relation

$$\dot{m} = \rho_c \frac{dl}{dt} \tag{B2}$$

Values for $\dot{m}$ appearing in equation (B1) may be obtained as follows:

An ablation rate $\dot{m}$ is assumed. For this assumed $\dot{m}$, the values of T_w and $c_{p,c}$ are obtained from figures 9 and 10 of reference 3. By using these values and the other required values as described in the next section, a modified enthalpy potential parameter and a heating rate are computed.

A value of h_{eff} which corresponds to this computed modified enthalpy potential parameter is read from figure 11. With this value of h_{eff} and the computed heating rate, an $\dot{m}$ is computed from the equation

$$\dot{m} = \frac{q}{h_{eff}} \tag{B3}$$

This computed $\dot{m}$ is compared with the assumed $\dot{m}$. If there is a difference the computed $\dot{m}$ is substituted for the assumed $\dot{m}$ and a second $\dot{m}$ is computed. The second computed $\dot{m}$ is compared with the second assumed $\dot{m}$, and so on, until equal values of $\dot{m}$ are obtained. Generally, two of these iterative processes are required to obtain an $\dot{m}$ which is accurate to within 5 percent. The values of $\dot{m}$ are computed as a function of time and plotted. Then equation (B1) is used to compute the ablated-length curves shown in figure 10.

An Explanation of Figures 11 and 12

The curve shown in figure 11 is reproduced from figure 8 of reference 3 and shows the effective heat of ablation plotted against the modified enthalpy potential parameter.

The modified enthalpy potential parameter appearing in figure 11 is a modification of the enthalpy potential computed from the following equation:

12

$$H_{aw} - H_w = \frac{V_\infty^2}{2gJ} + c_{p,\infty}T_\infty - c_{p,c}T_w \qquad (B4)$$

where

$2gJ$ energy conversion factor, assumed to be equal to 50,000

T_∞ free-stream temperature of air as a function of altitude, obtained
from standard charts of atmosphere

$c_{p,\infty}$ specific heat at constant pressure of air as a function of T_∞
obtained from tables of properties of gases (ref. 9)

T_w ablating wall temperature of Teflon, obtained from curve of T_w as
a function of $\dot{m}$ shown in figure 9 of reference 3 or in figure 4
of reference 10.

In the method of reference 10 the Teflon ablating surface is assumed to be a
burning surface and the surface temperature to be essentially the burning tem-
perature. The surface temperature is thus dependent on the burning rate, or
what would be the ablation rate in the case of ablating materials, and the mate-
rial properties such as density, thermal conductivity, and specific heat.

The specific heat at constant pressure $c_{p,c}$ represents that of the Teflon
vapor. It is assumed that Teflon vapor consists of C_2F_4 molecules having a
molecular weight of approximately 100. A curve of specific heat plotted against
temperature for this vapor state is given in figure 10 of reference 3. The
vapor temperature is assumed to be equal to the surface temperature or the
Teflon ablating wall temperature.

Other parameters in the modified enthalpy potential parameter are

T_l air temperature behind strong bow shock, obtained from compressible
flow tables for air

$c_{p,l}$ specific heat at constant pressure of air as a function of T_l,
obtained from charts of properties of air (ref. 9) or computed from

$$c_{p,l} = \frac{H_l - H_w}{T_l - T_w} \quad \text{for values of} \quad T_l \quad \text{above } 4,000^\circ \text{ F}$$

H_l local enthalpy, obtained from charts of thermodynamic properties of
high-temperature air

Normally $c_{p,c}$ and T_w are obtained as functions of $\dot{m}$ from figures 9
and 10 of reference 3.

The effective heat of ablation parameter appearing in figure 11 is defined
as the net aerodynamic heating rate (calculated at the temperature of the
ablating surface) divided by the rate of ablation. (See eq. (B3).) The values

13

of $\dot{m}$ in equation (B3) are determined by using equation (B2) with the results of earlier experimental measurements.

Figure 12(a) shows the heating rates q at sensors 2 and 3. These heating rates were identical as a result of the model surface geometry and they were computed from the following empirical formula of reference 11 (in the notation of the present paper):

$$q = \frac{17,600}{\sqrt{r}} \sqrt{\frac{p_\infty}{p_{sl}}} \left(\frac{V_\infty}{26,000} \right)^{3.15} \frac{H_{aw} - H_w}{H_{aw} - (H_w)_{300^\circ \text{ K}}} \tag{B5}$$

The heating rates from this relationship are for the stagnation point on a hemisphere. Therefore, they were multiplied by 0.71 in order to correct them for the effects of bluntness according to figure 3 of reference 12.

Figure 12(b) shows the range of theoretical h_{eff} obtained from figure 11 and used in equation (B3).

14

REFERENCES

1. Roberts, Leonard: A Theoretical Study of Stagnation-Point Ablation. NASA TR R-9, 1959. (Supersedes NACA TN 4392.)

2. Rashis, Bernard, and Walton, Thomas E., Jr.: An Experimental Investigation of Ablating Materials at Low and High Enthalpy Potentials. NASA TM X-263, 1960.

3. Rashis, Bernard, and Hopko, Russell N.: An Analytical Investigation of Ablation. NASA TM X-300, 1960.

4. Winters, Clyde W., Witte, William G., Rashis, Bernard, and Hopko, Russell N.: A Free-Flight Investigation of Ablation of a Blunt Body to a Mach Number of 13.1. NASA TN D-1500, 1962.

5. Winters, Clyde W., and Bracalente, Emedio M.: A Sensor for Obtaining Ablation Rates. NASA TN D-800, 1960.

6. Hill, P. R.: A Method of Computing the Transient Temperature of Thick Walls From Arbitrary Variation of Adiabatic-Wall Temperature and Heat-Transfer Coefficient. NACA Rep. 1372, 1958. (Supersedes NACA TN 4105.)

7. Van Driest, E. R.: The Problem of Aerodynamic Heating. Aero. Eng. Rev., vol. 15, no. 10, Oct. 1956, pp. 26-41.

8. Swann, Robert T., and Pittman, Claud M.: Numerical Analysis of the Transient Response of Advanced Thermal Protection Systems for Atmospheric Entry. NASA TN D-1370, 1962.

9. Anon.: U.S. Standard Atmosphere, 1962. NASA, U.S. Air Force, and U.S. Weather Bureau, Dec. 1962.

10. Steg, Leo: Materials for Re-Entry Heat Protection of Satellites. ARS Jour., vol. 30, no. 9, Sept. 1960, pp. 815-822.

11. Detra, R. W., Kemp, N. H., and Riddell, F. R.: Addendum to "Heat Transfer to Satellite Vehicles Re-entering the Earth's Atmosphere." Jet Propulsion, vol. 27, no. 12, Dec. 1957, pp. 1256-1257.

12. Stoney, William E., Jr.: Aerodynamic Heating of Blunt Nose Shapes at Mach Numbers up to 14. NACA RM L58E05a, 1958.

Figure 1.- Photograph of model.

L-60-4532
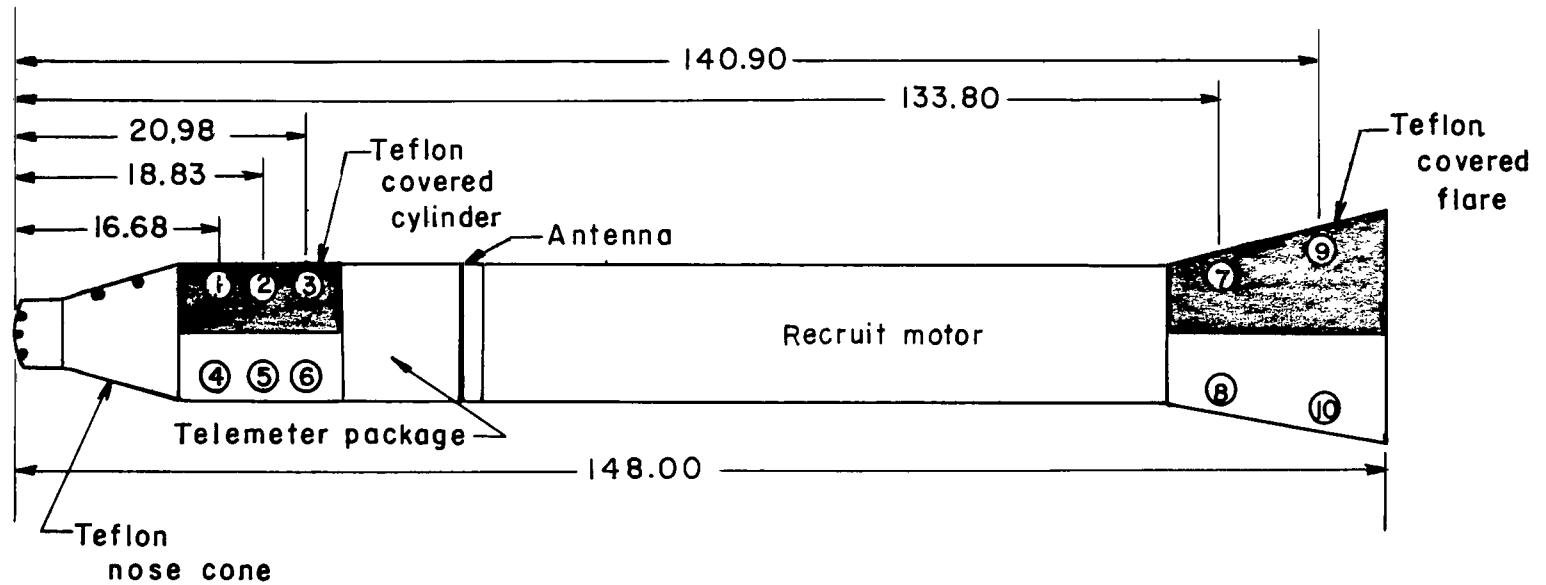
Figure 2.- Drawing of model. All dimensions are in inches.

Teflon
ablation sensors

Magnesium
insert

10°

5.6

3

1.12

5

4

3

2

4.0

12°

Center of radius of
curvature 6.0

9.0

1

.75

Teflon nose

9.10
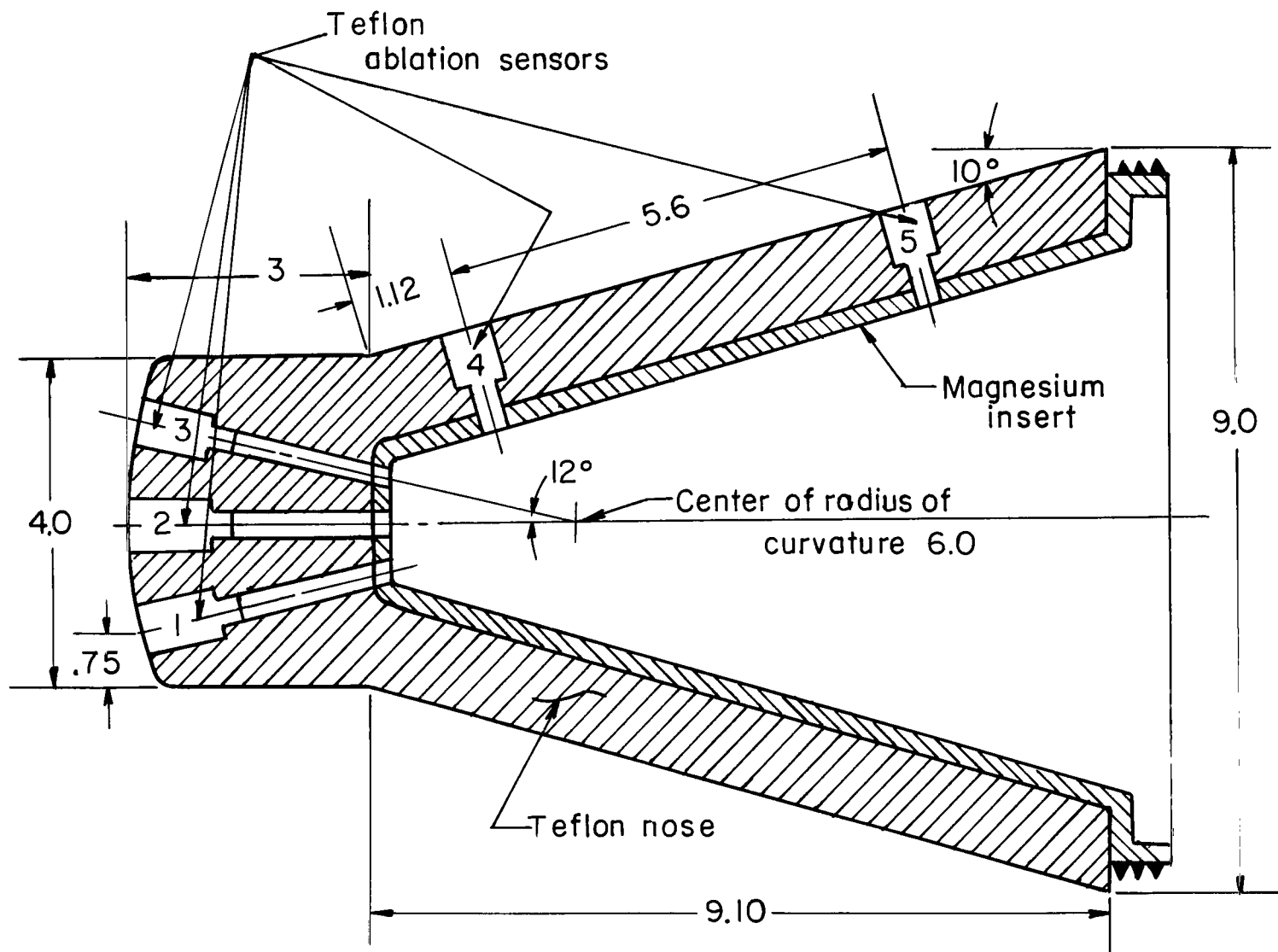
Figure 3.- Details of model nose. All dimensions are in inches.
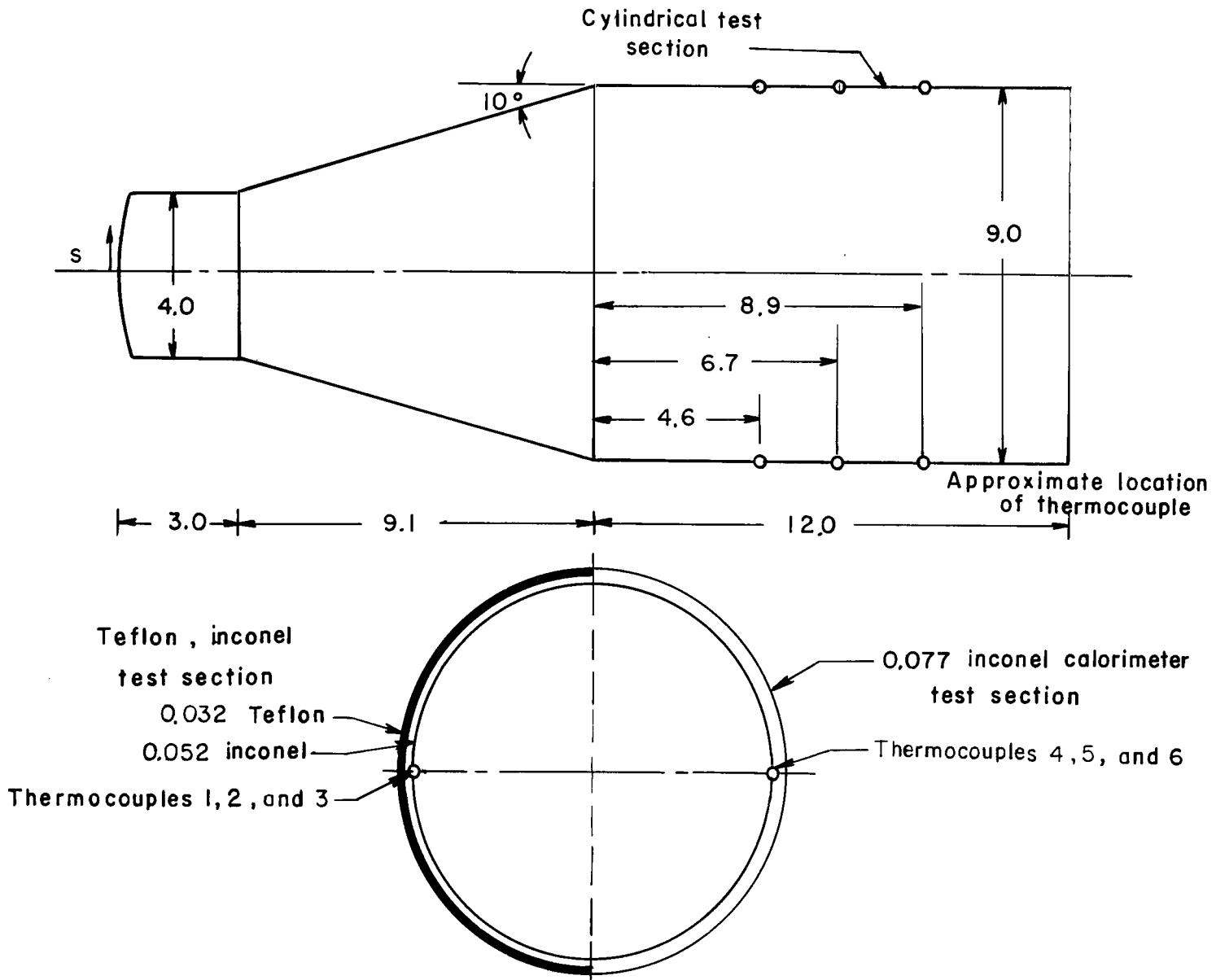
Figure 4.- Drawing of cylindrical section, showing thermocouple locations. All dimensions are in inches.
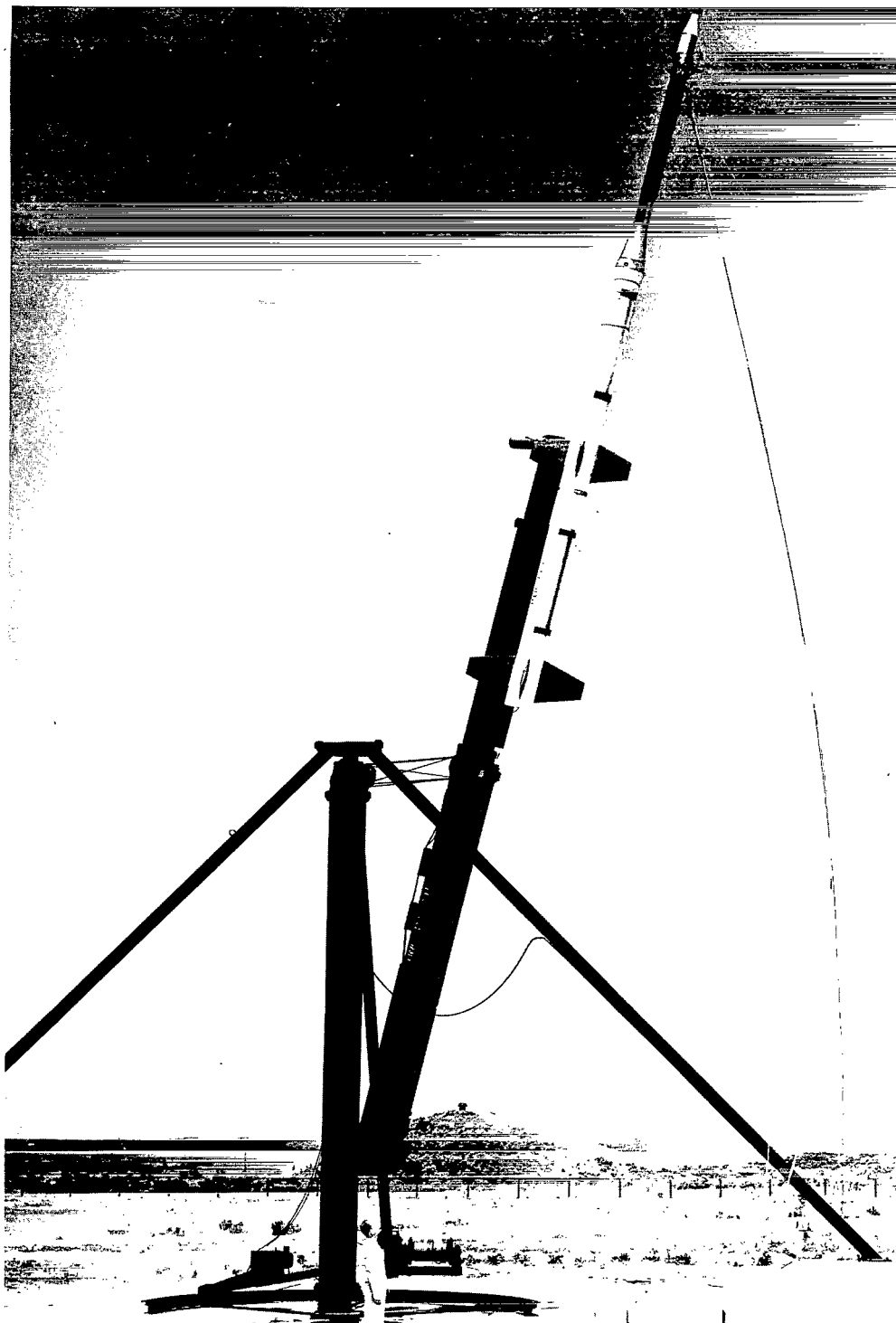
L-60-4526

Figure 5.- Photograph of model and boosters in launch position.

20
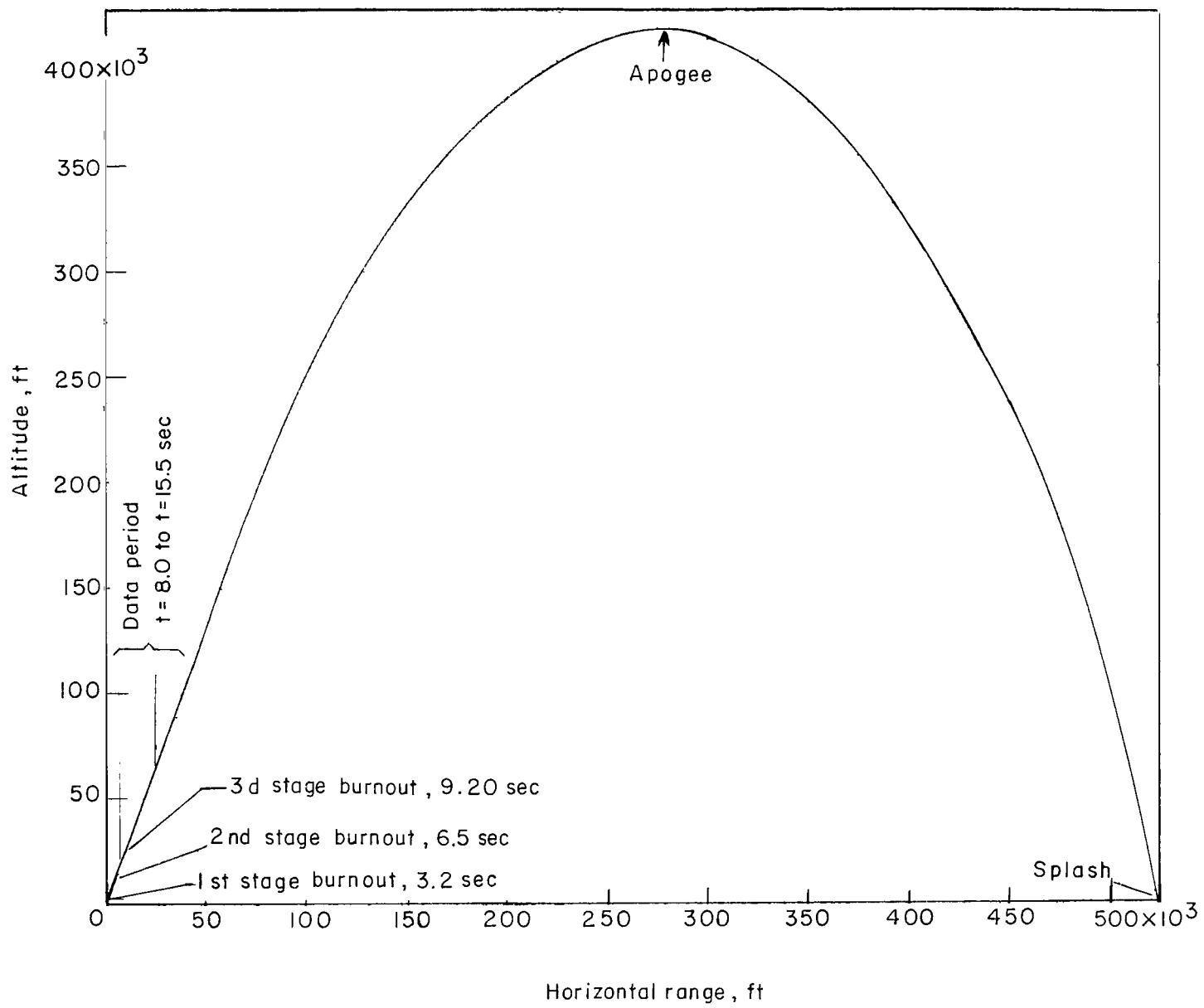
Figure 6.- Flight trajectory.
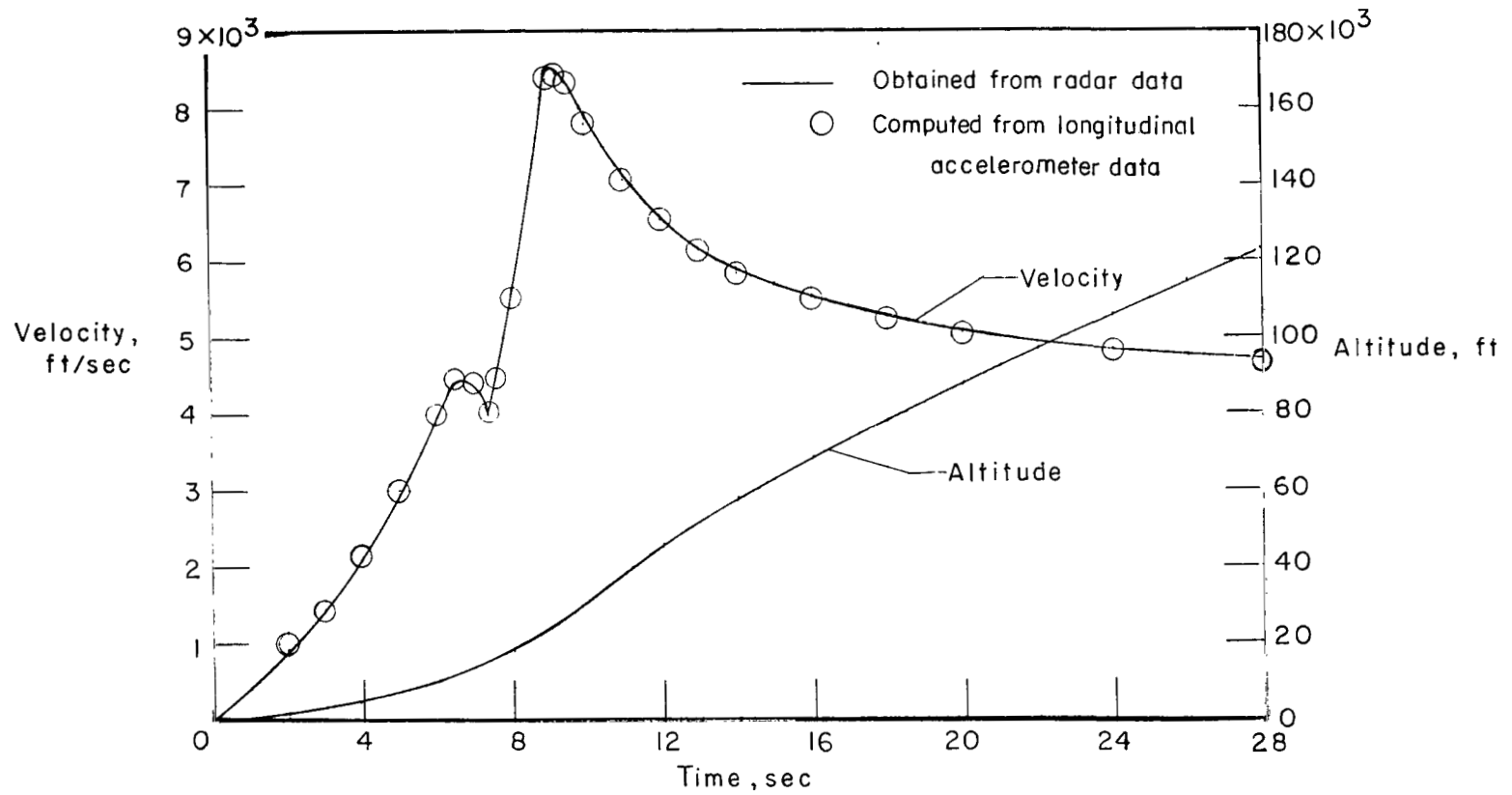
Figure 7.- Time histories of velocity and altitude.
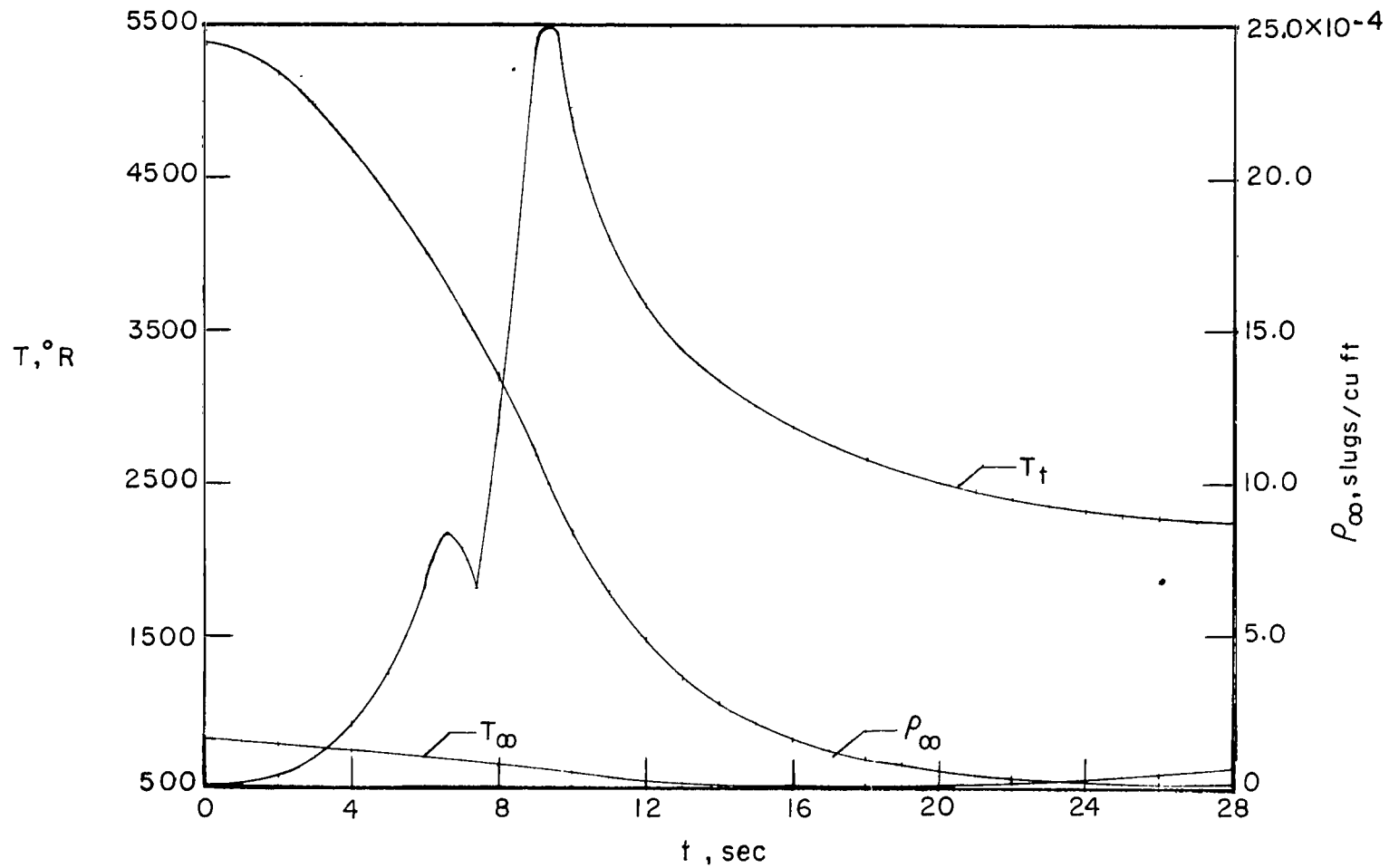
Figure 8.- Time histories of ambient conditions and calculated stagnation temperature.
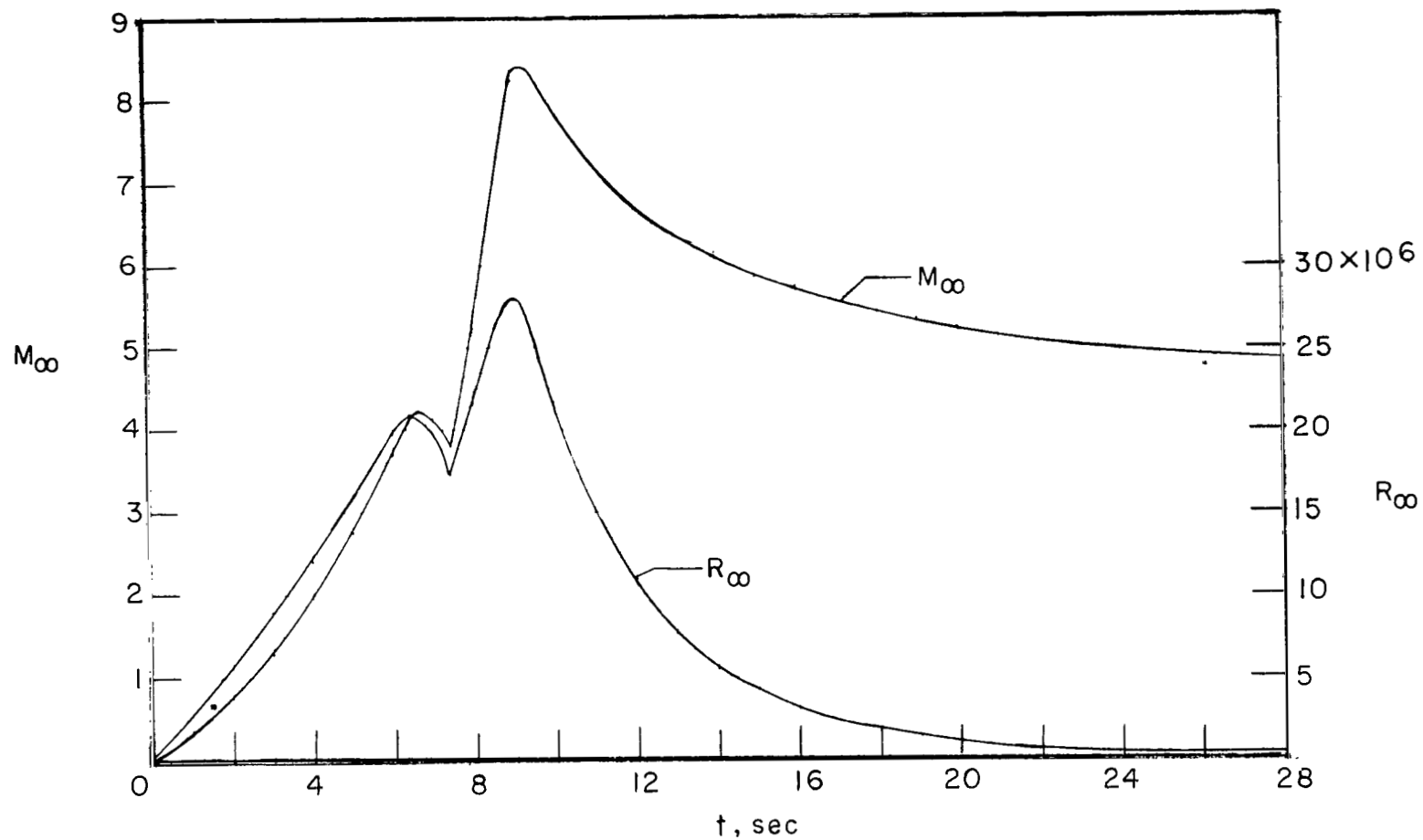
Figure 9.- Time histories of free-stream Mach number and free-stream Reynolds number per foot.
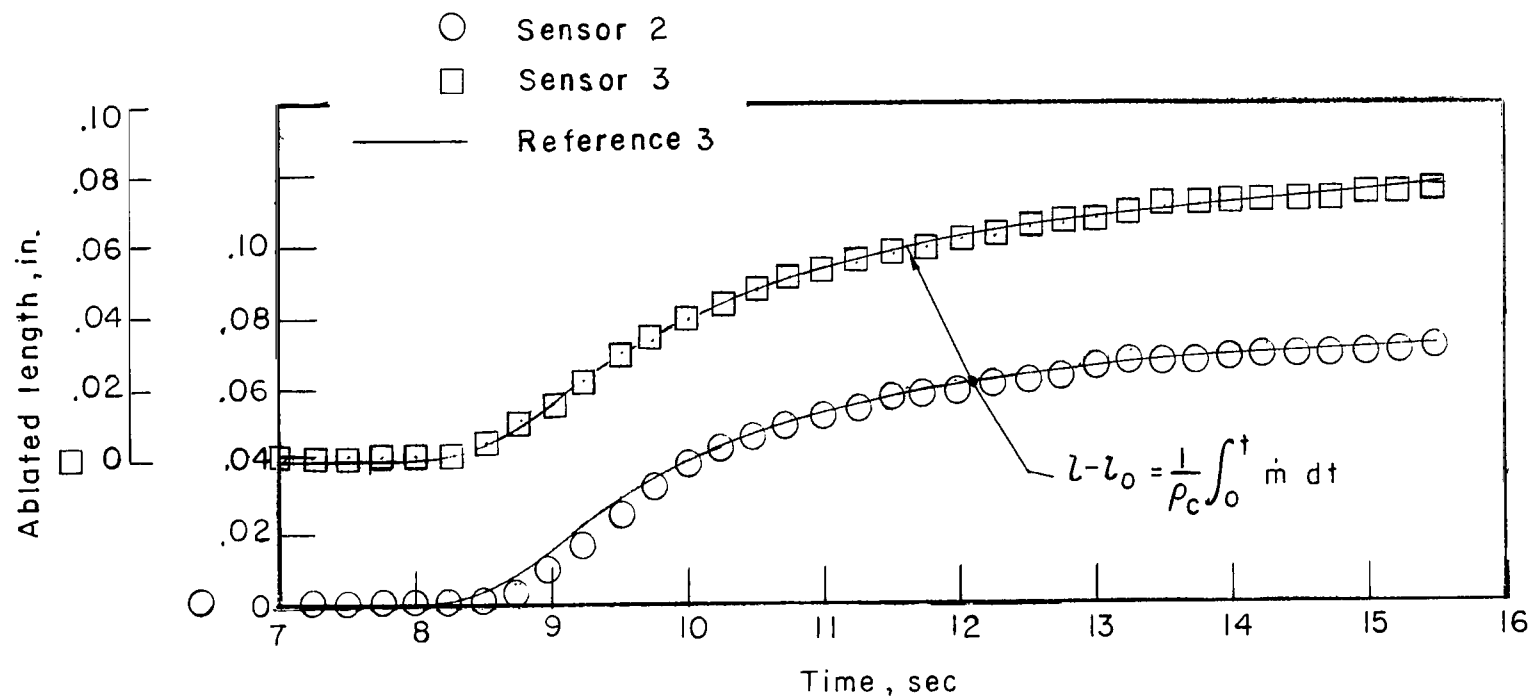
Figure 10.- Time histories of ablated lengths for ablation sensors 2 and 3.

The chart shows:

Legend:
- ○ Sensor 2
- □ Sensor 3
- —— Reference 3

Y-axis (left): Ablated length, in.

Equation annotation:

$$l - l_0 = \frac{1}{\rho_c} \int_0^t \dot{m}\, dt$$

X-axis: Time, sec
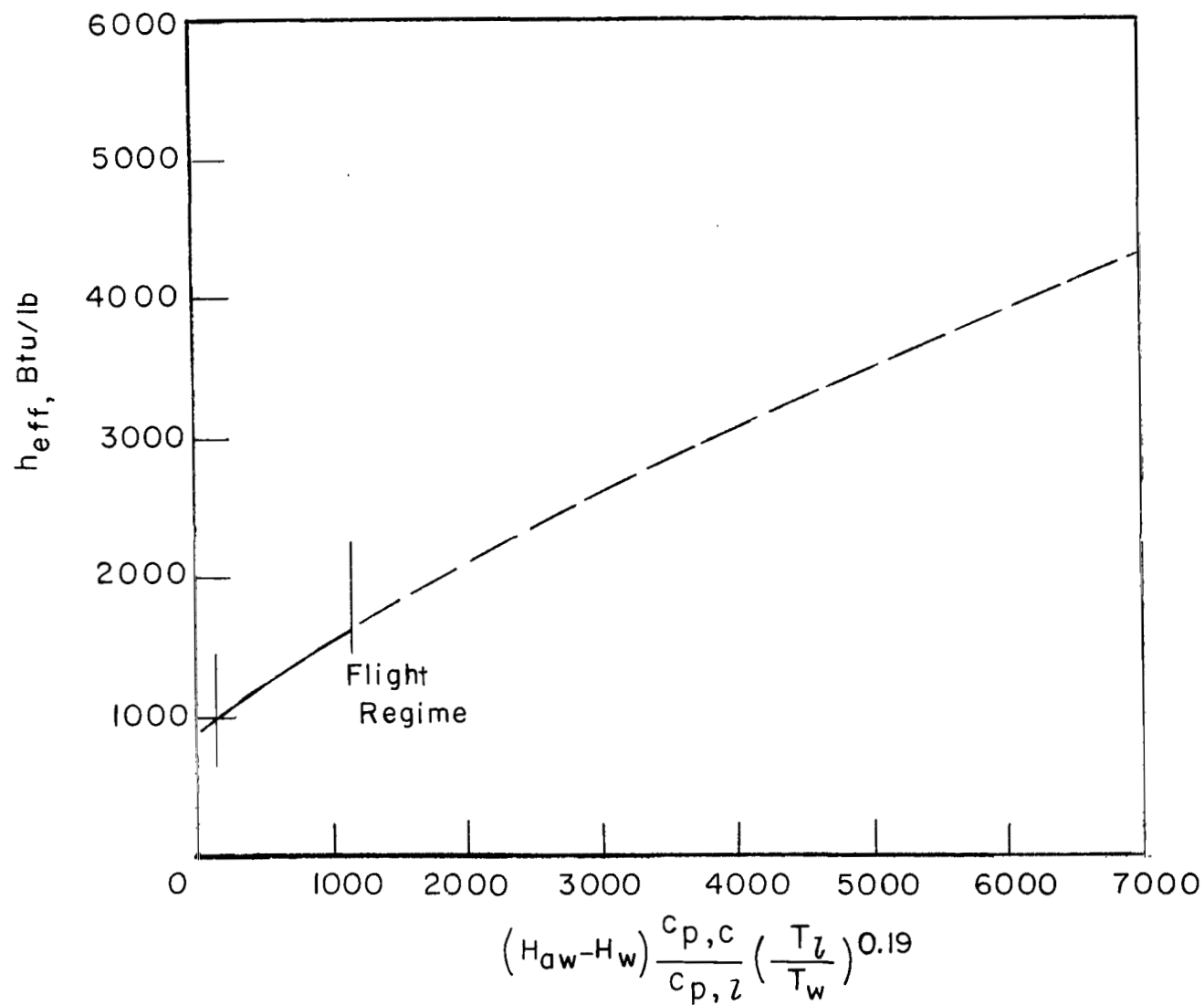
Figure 11.- Predicted effectiveness of Teflon material (based on data from ref. 3).
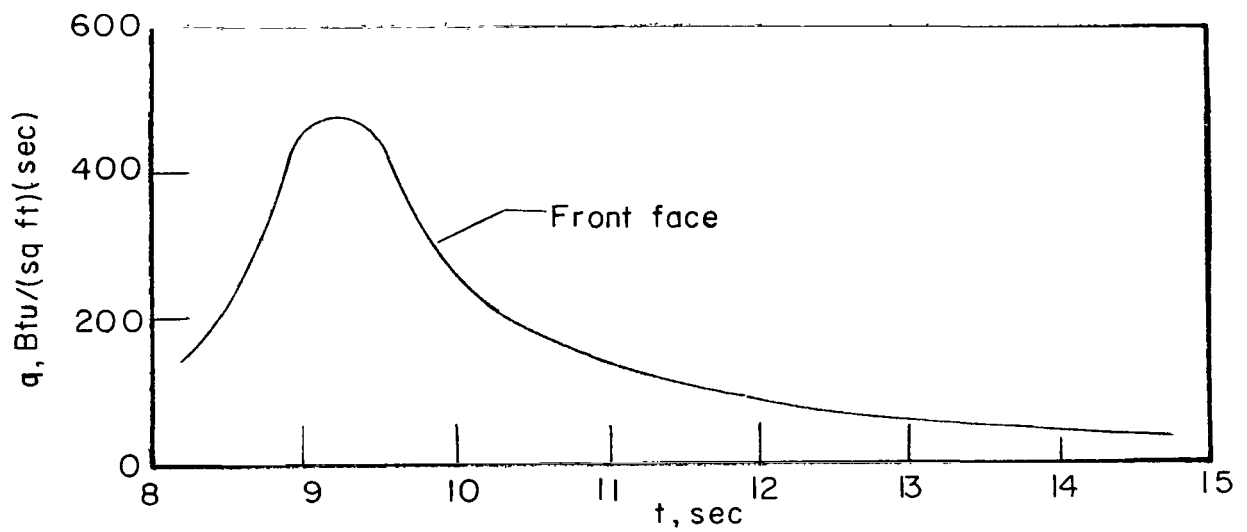
(a) Heating rates.
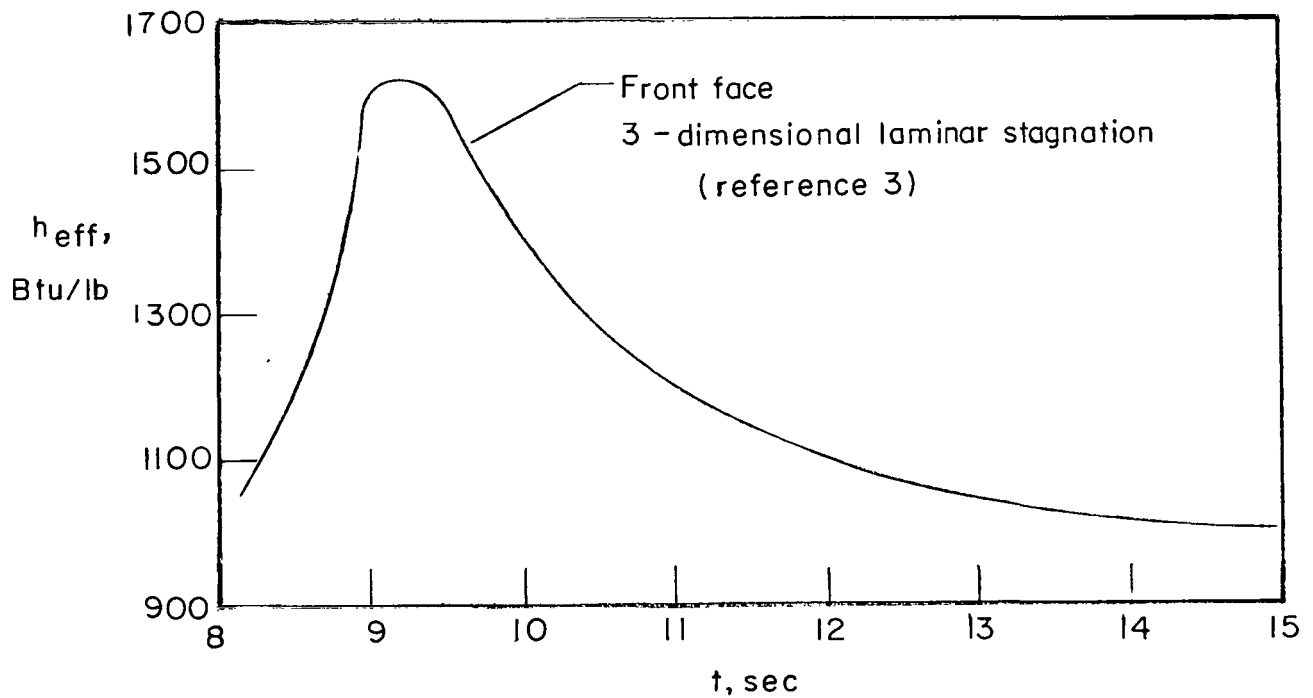
(b) Effective heats of ablation for test.

Figure 12.- Theoretical effective heats of ablation and heating rates calculated for nose sensors.

27
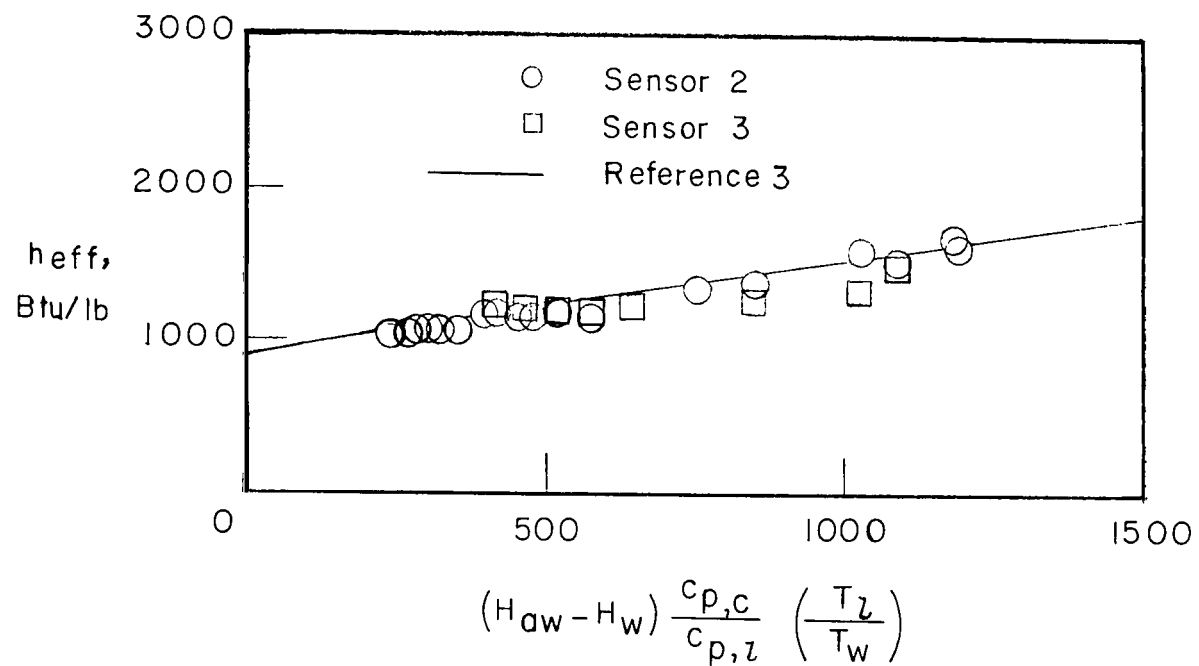
Figure 13.- Comparison of flight data with predicted effectiveness of Teflon for three-dimensional laminar stagnation point case (data from ref. 3).

Thermocouple I (under 0.052-inch inconel and
0.032-inch Teflon)

Thermocouple 4 (under 0.077-inch inconel)
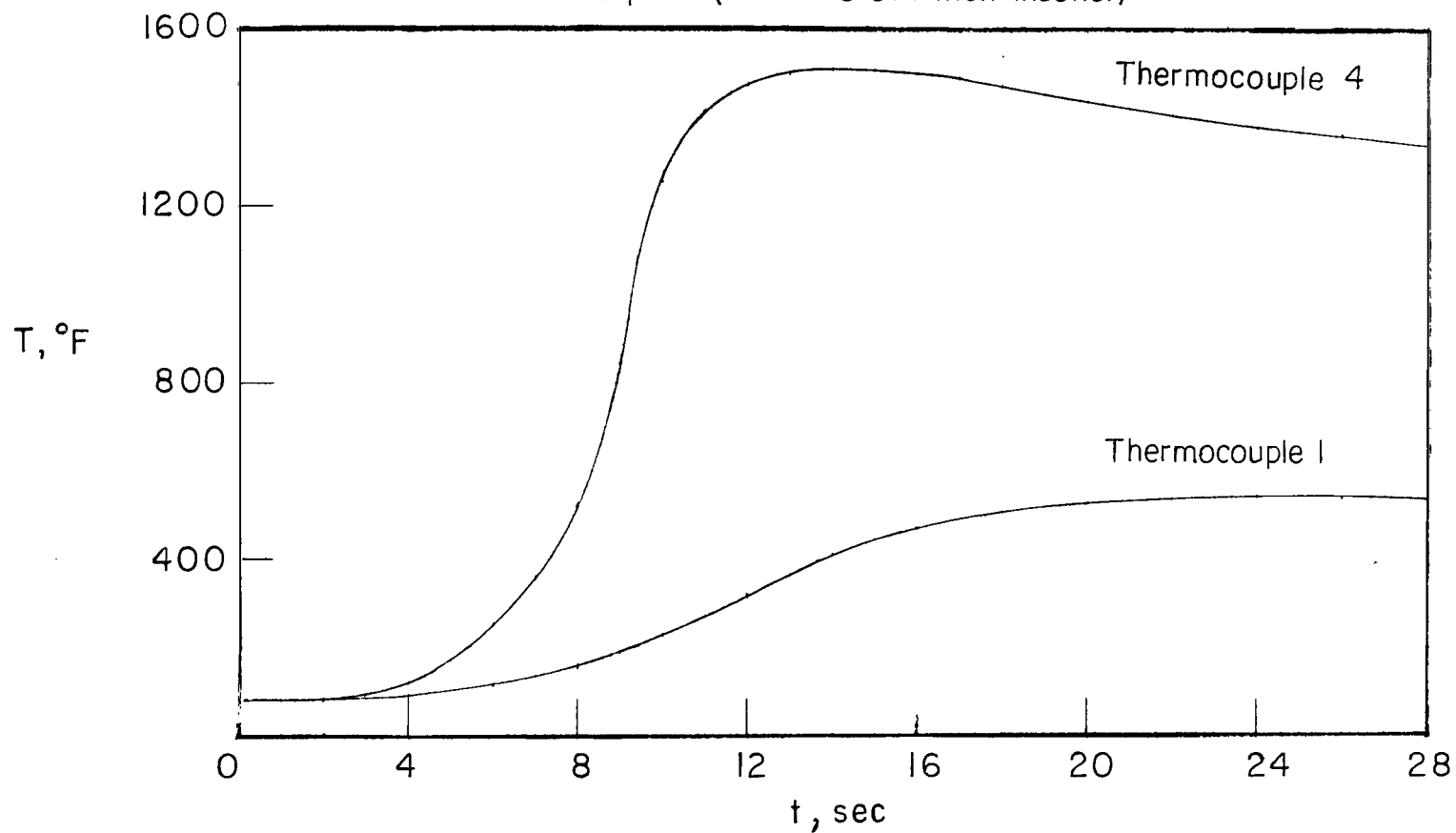
(a)   s = 19.0 inches.

Figure 14.- Inside wall temperature along cylinder.

Thermocouple 2 (under 0.052-inch inconel and 0.032-inch Teflon)

Thermocouple 5 (under 0.077-inch inconel)
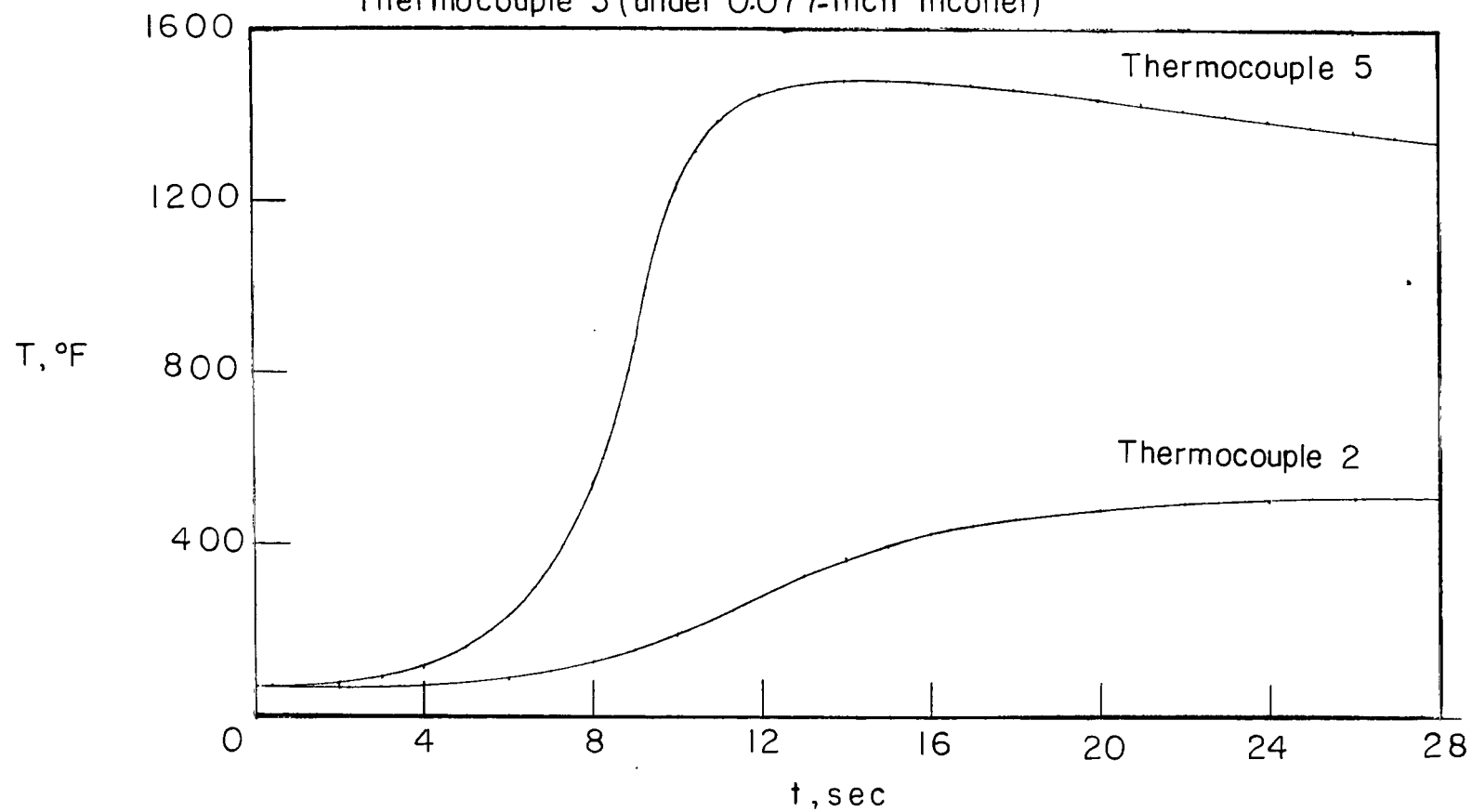
(b)   s = 21.0 inches.

Figure 14.- Continued.

Thermocouple 3 (under 0.052-inch inconel and 0.032-inch Teflon)

Thermocouple 6 (under 0.077-inch inconel)
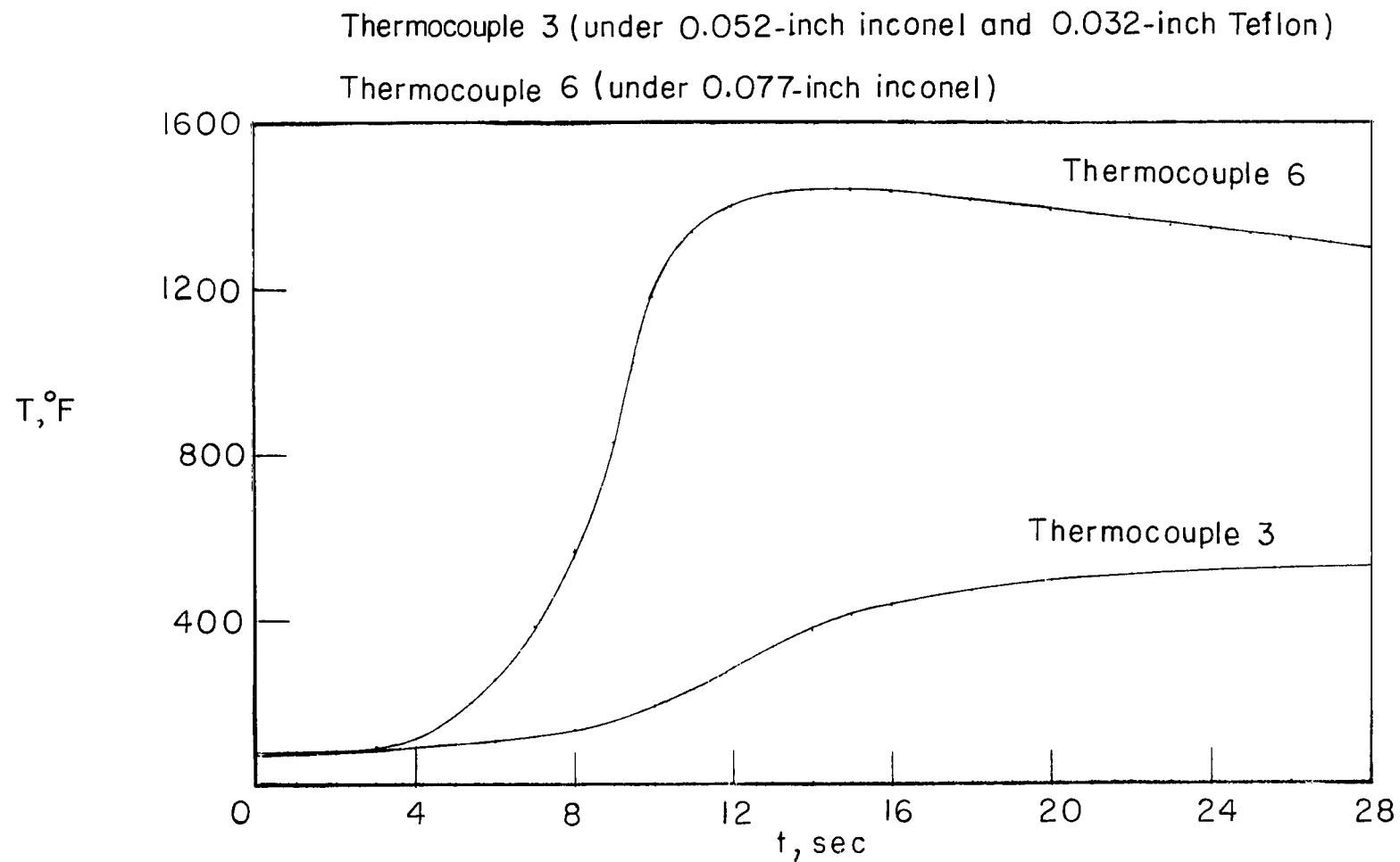
(c) s = 23.0 inches.

Figure 14.- Concluded.
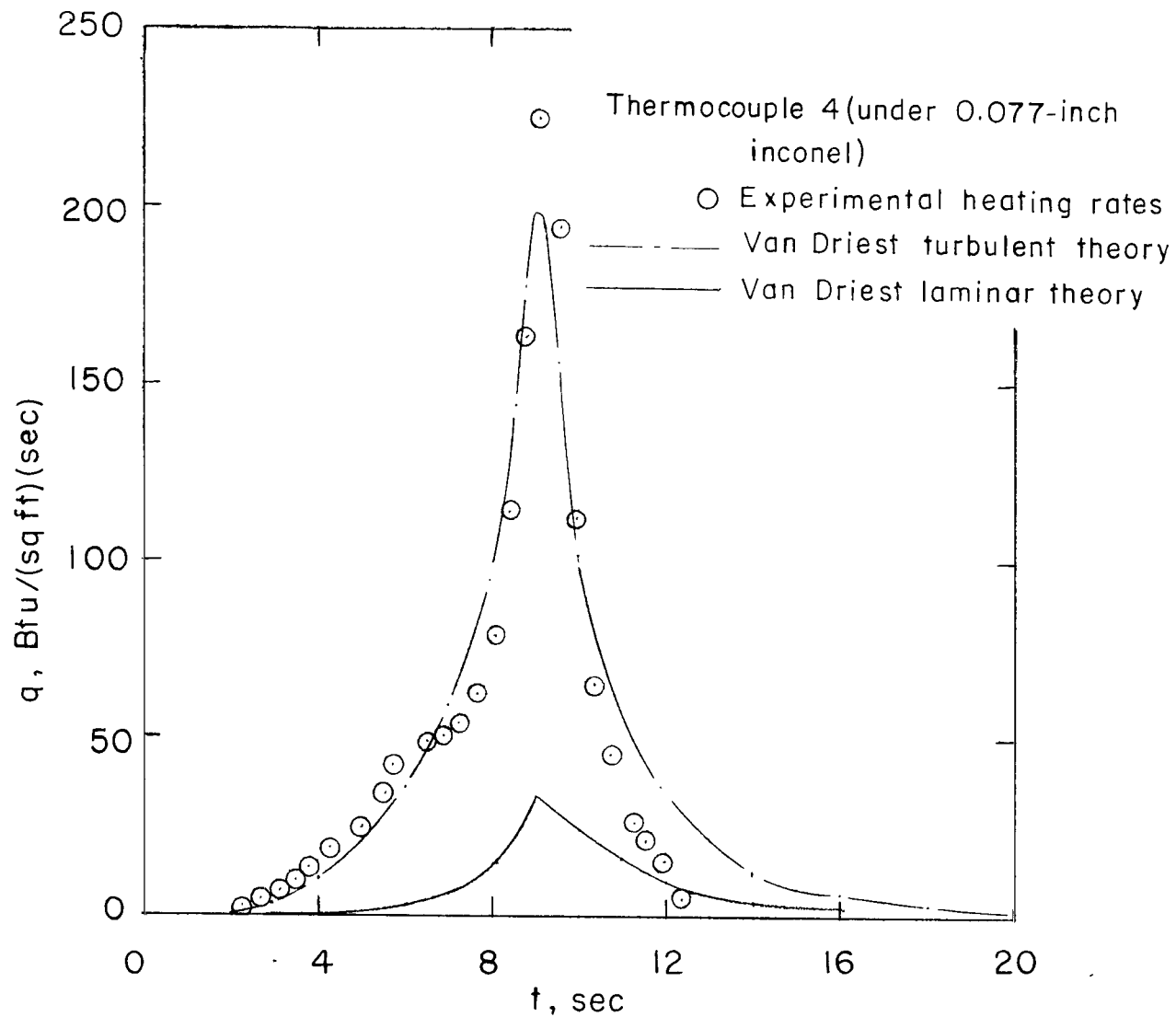
(a) s = 19.0 inches.

Figure 15.- Comparison of experimental heating rates with Van Driest turbulent and laminar flat-plate theory.
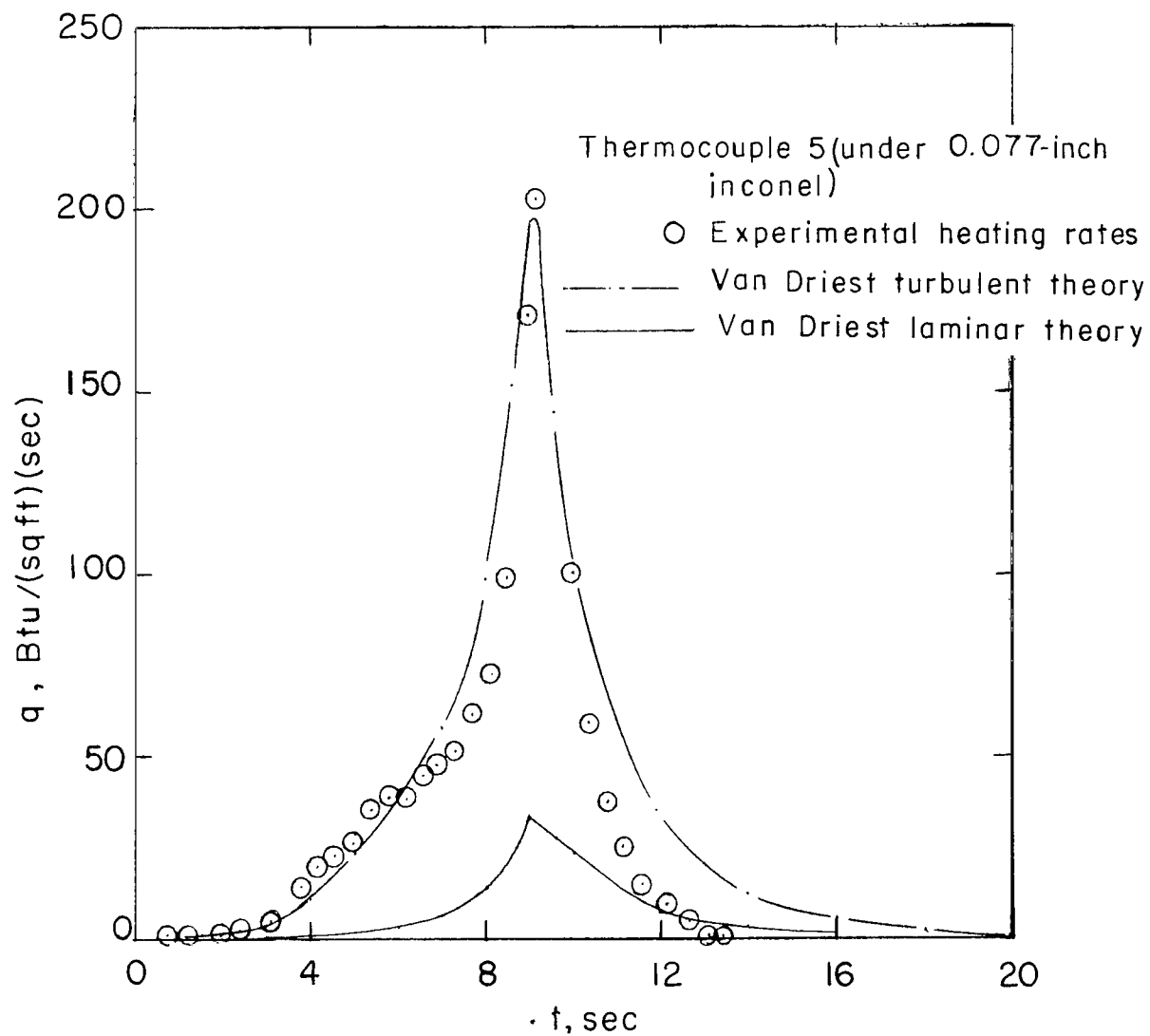
(b) s = 21.0 inches.

Figure 15.- Continued.

34
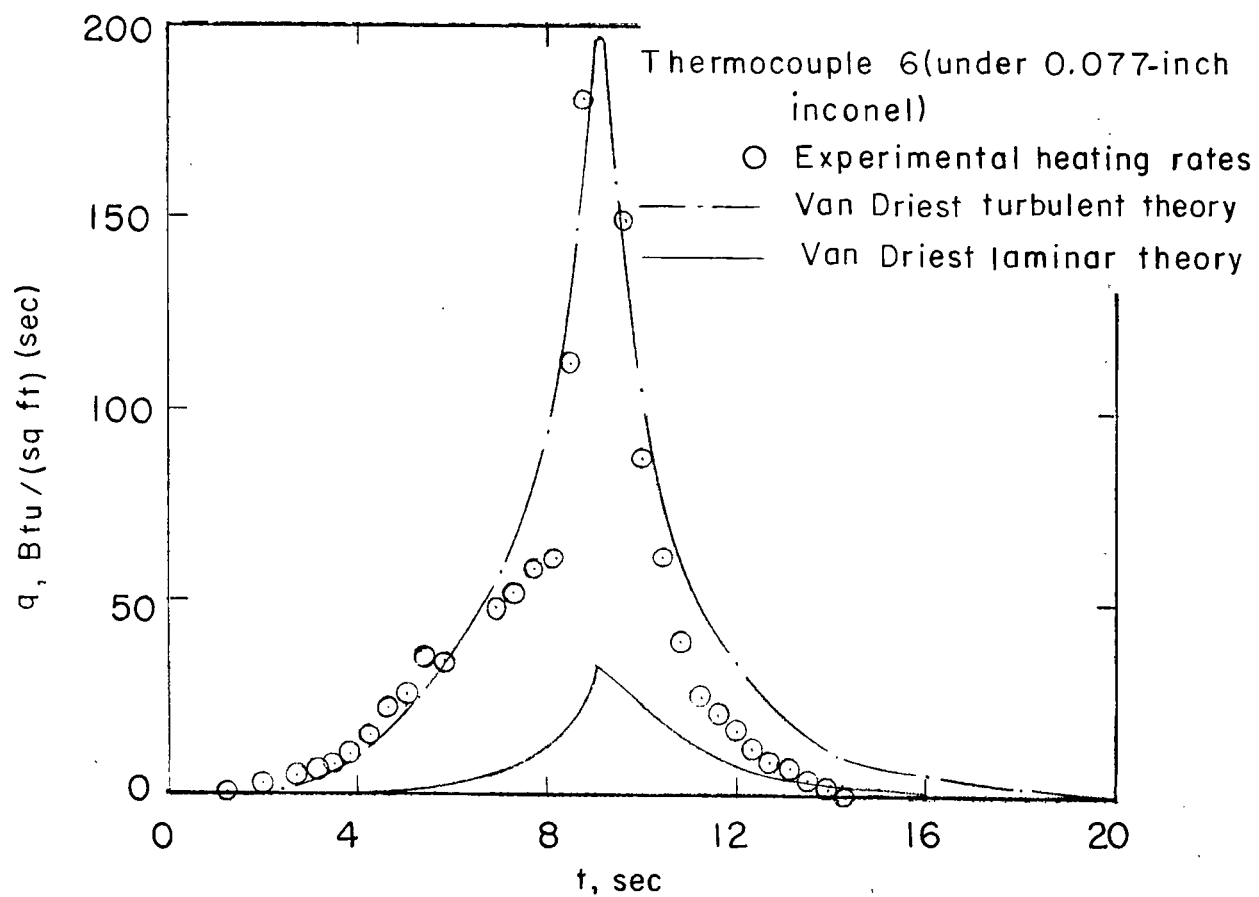
(c) s = 23.0 inches.

Figure 15.- Concluded.
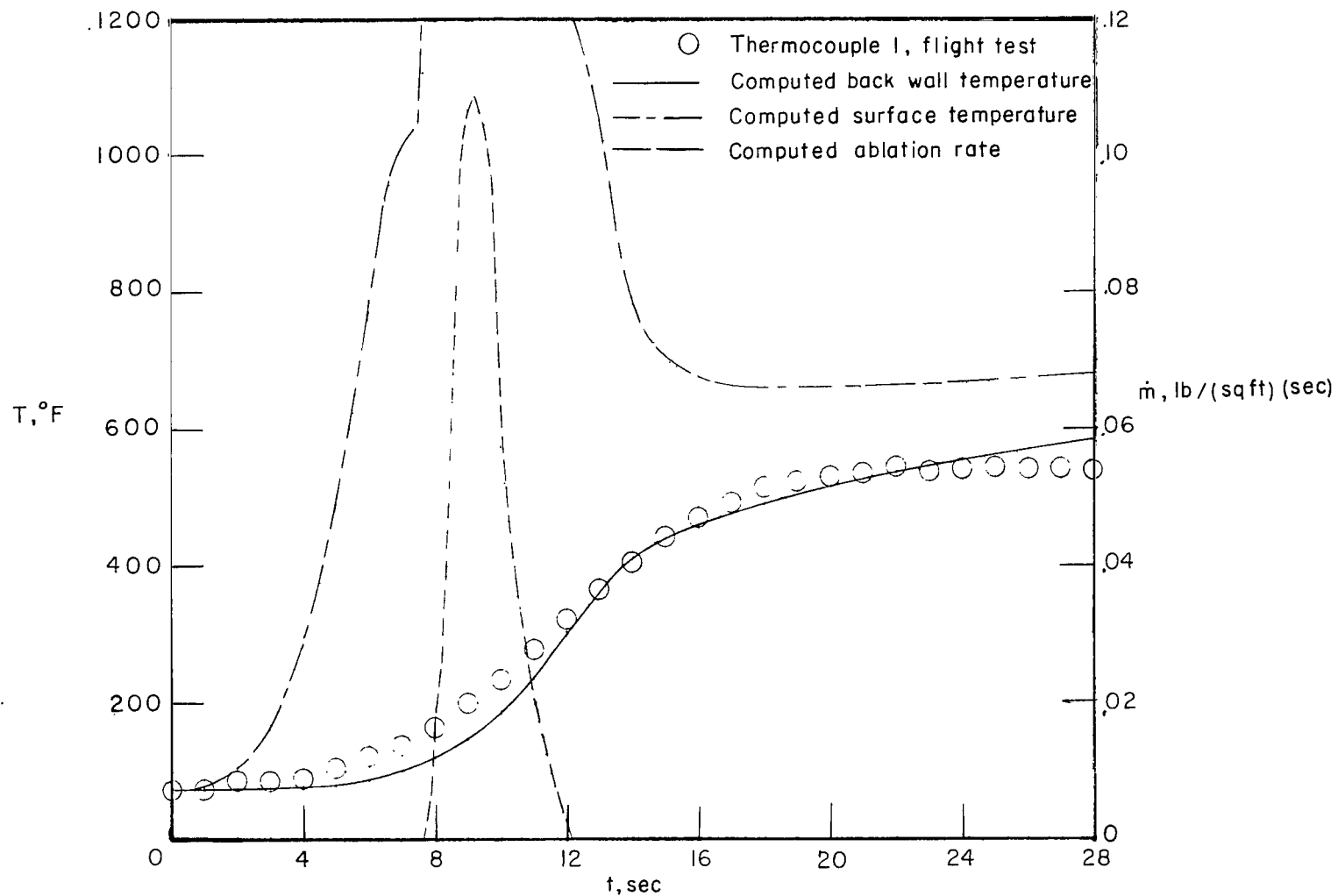
(a)   s = 19.0 inches.

Figure 16.- Computed Teflon surface temperature history (assuming a constant ablation temperature of 1,200° F), computed inconel back wall temperature history, measured inconel back wall temperature history, and computed albation rate.
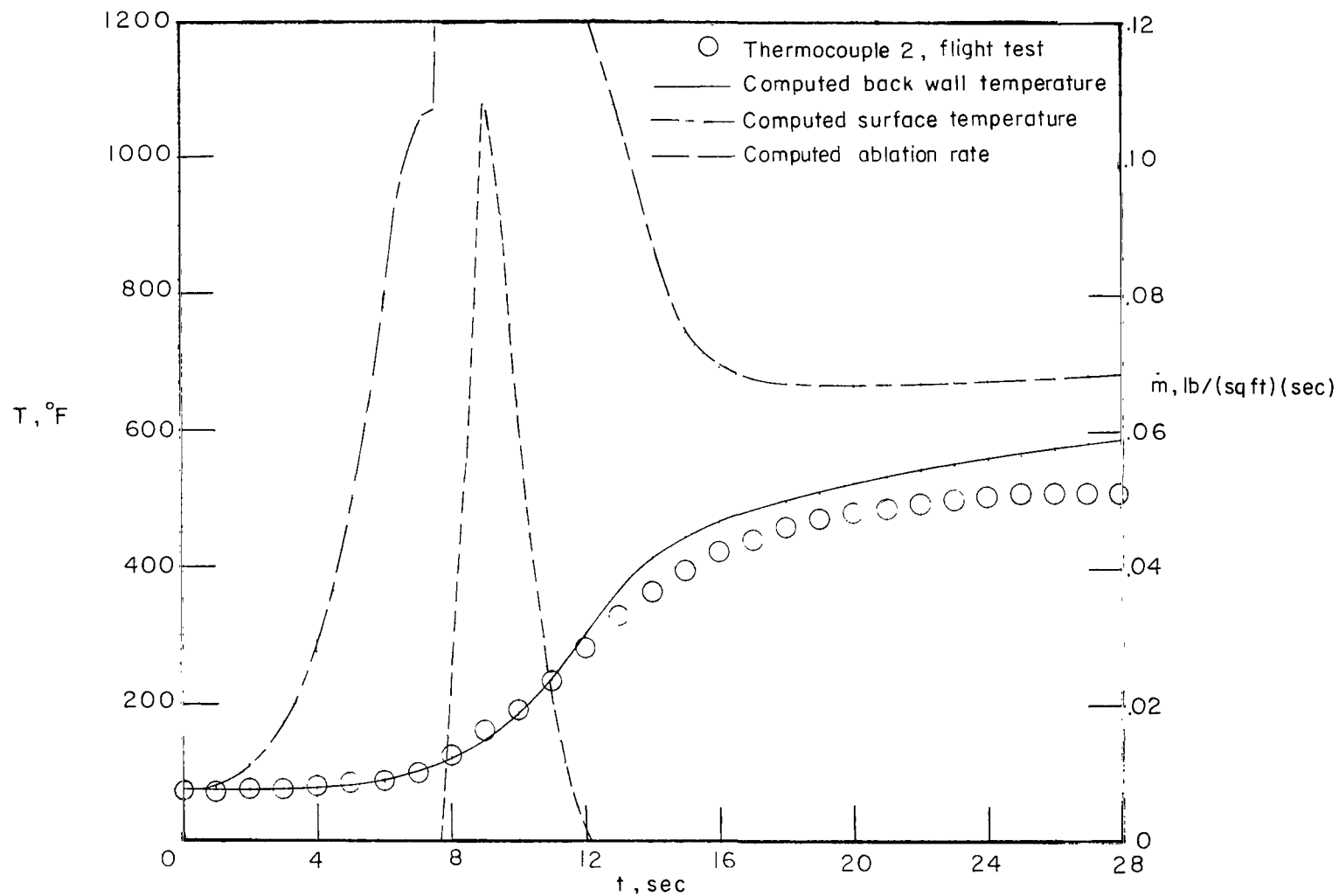
(b) s = 21.0 inches.

Figure 16.- Continued.
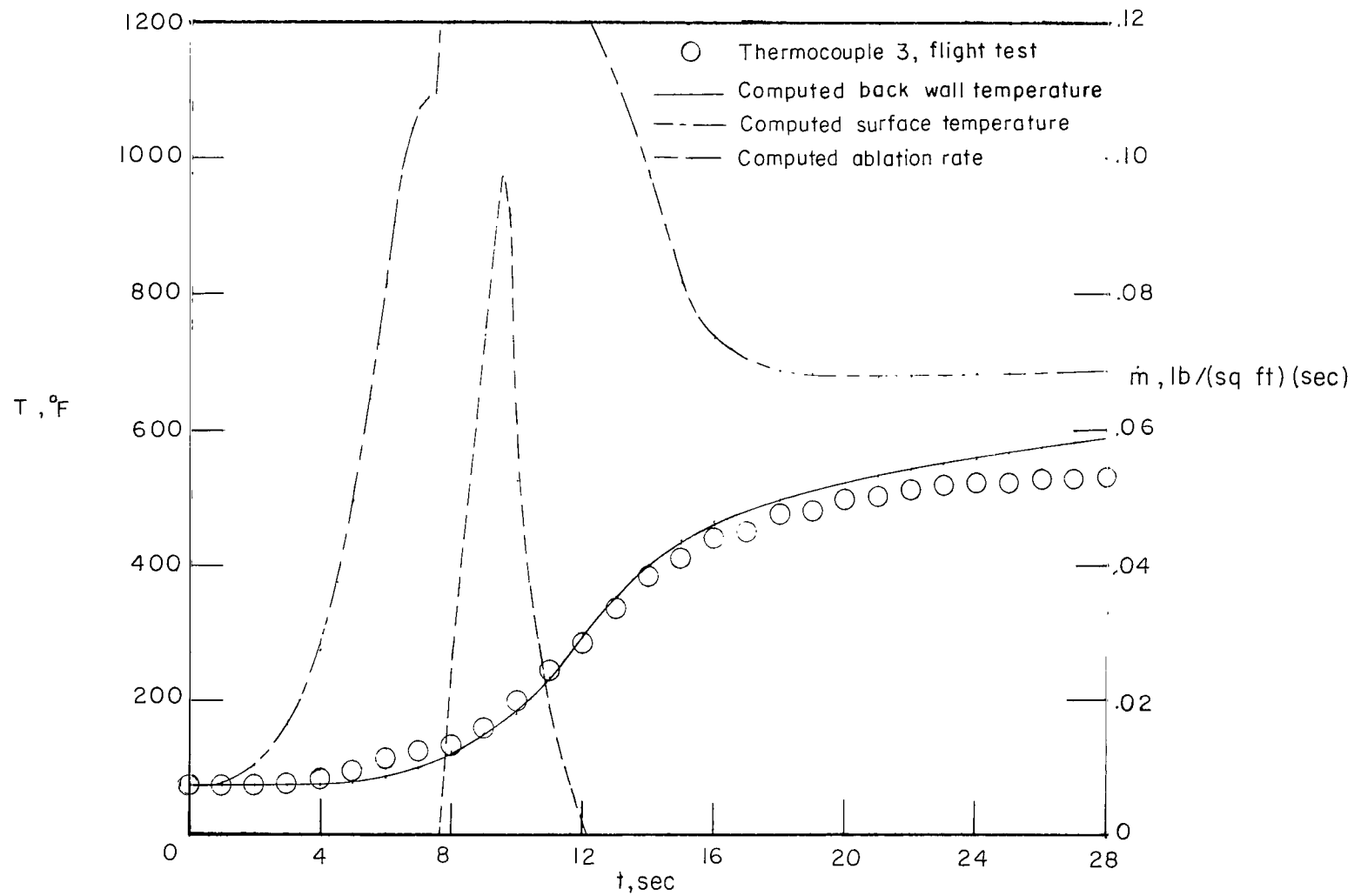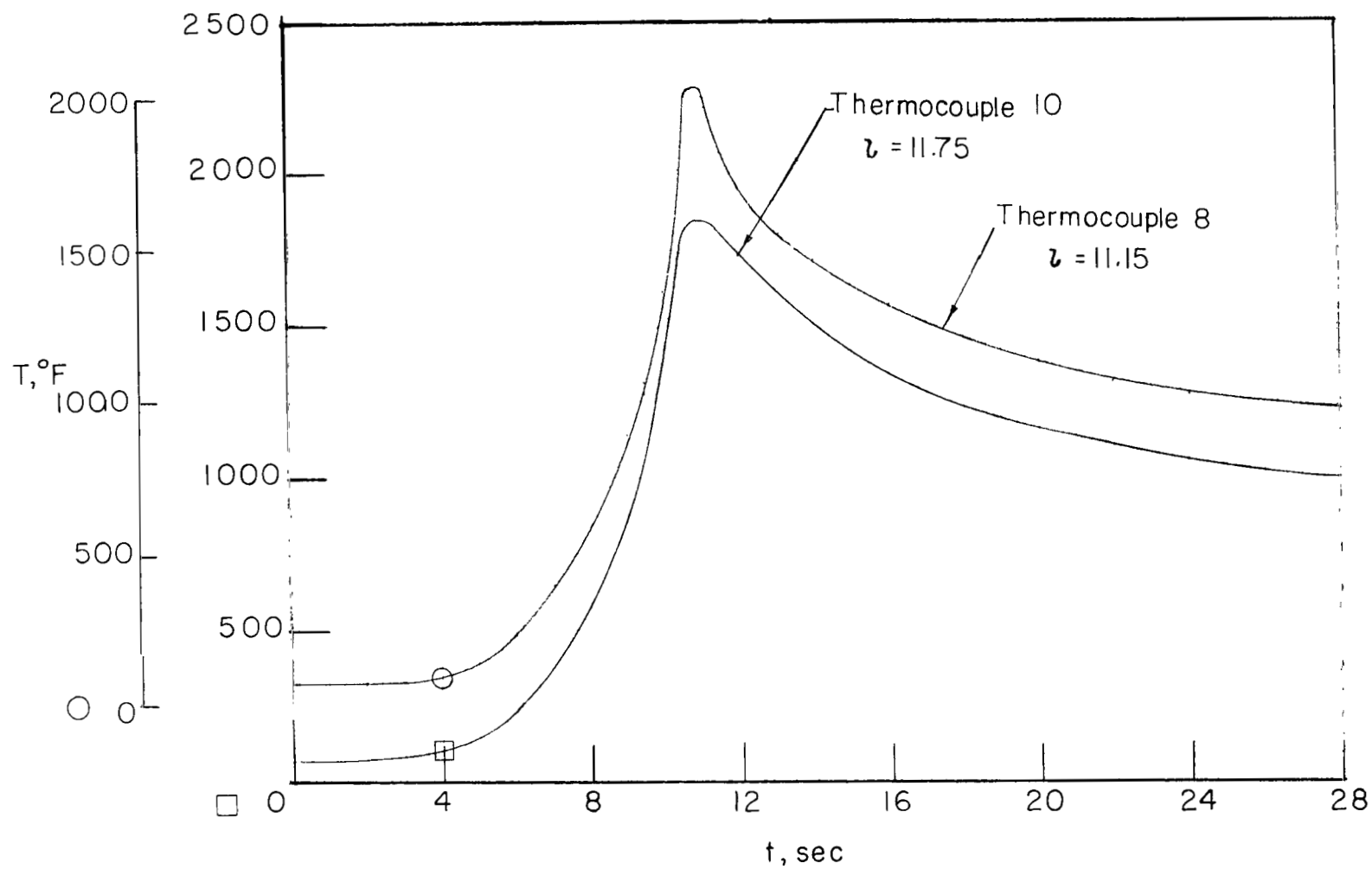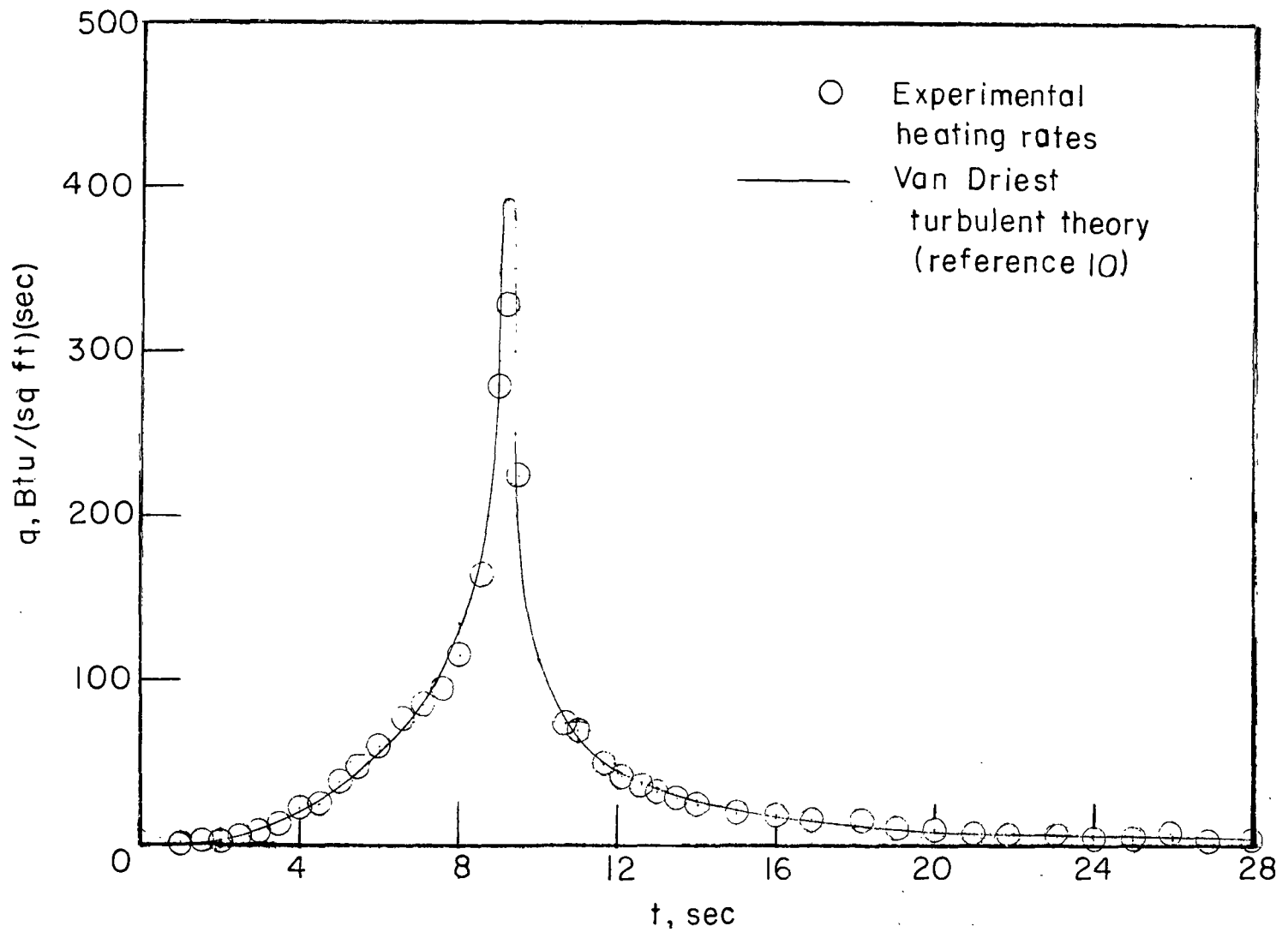
(c)   s = 23.0 inches.
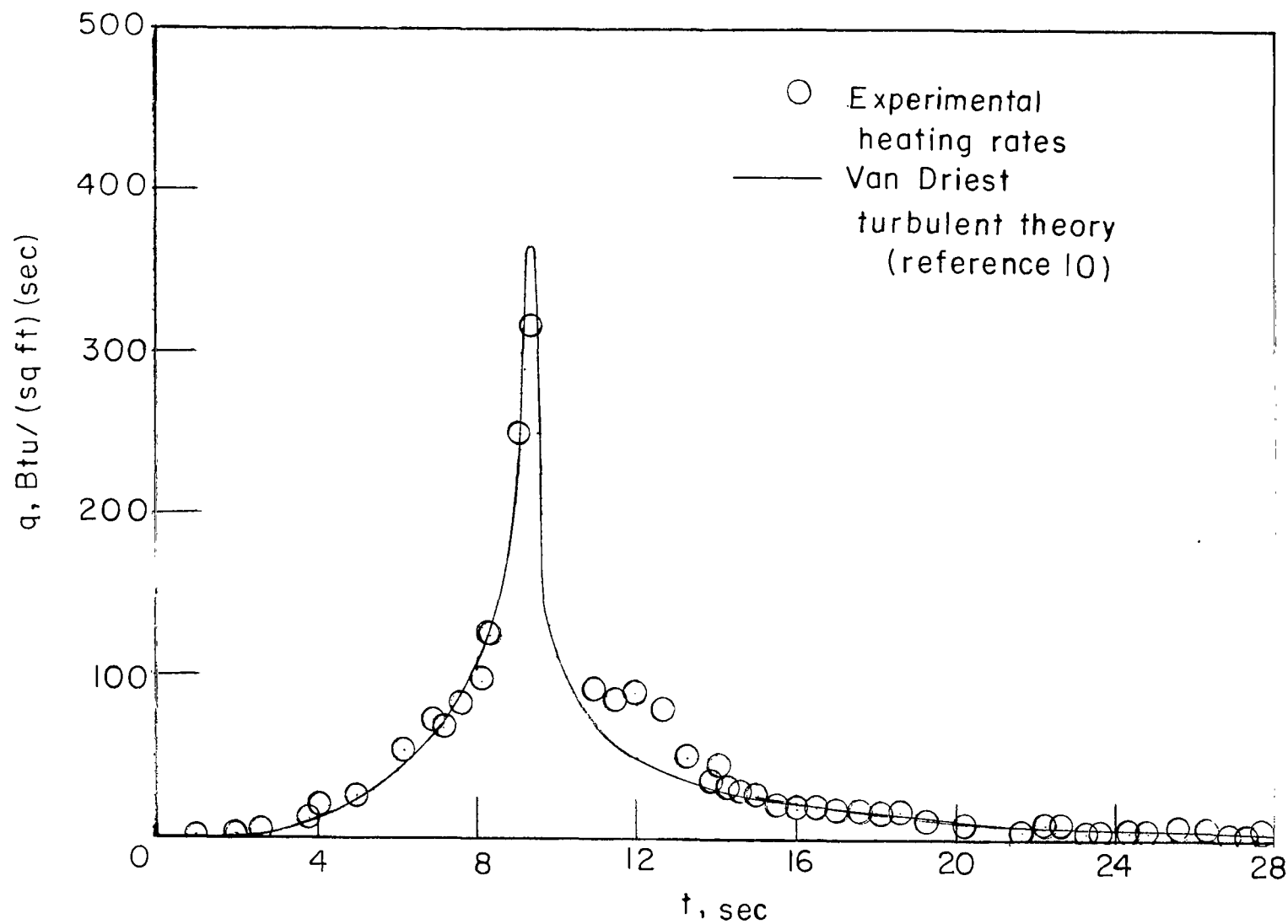
Figure 16.- Concluded.

Figure 17.- Faired inside wall temperatures along calorimeter portion of model flare.

(a) Thermocouple 8.

Figure 18.- Comparison of experimental heating rates with Van Driest turbulent theory.

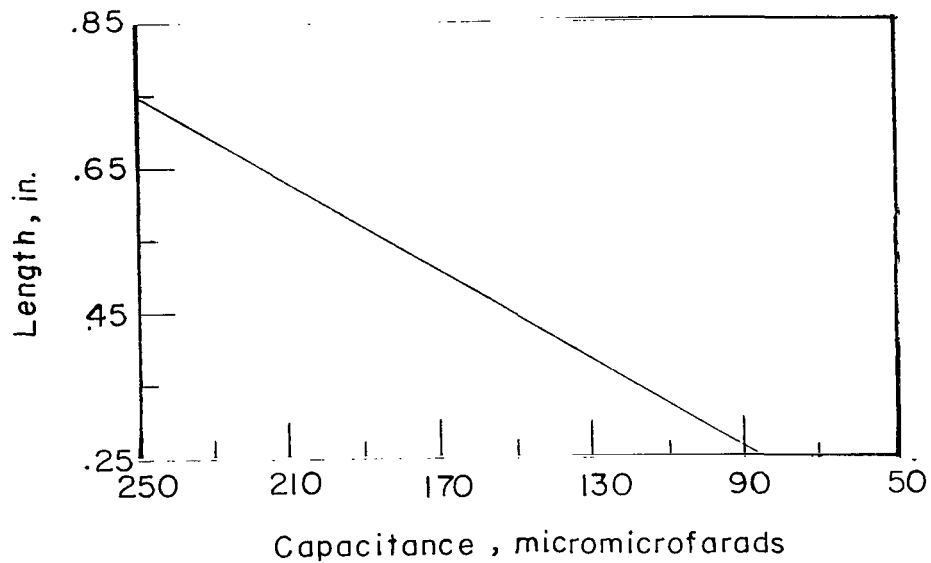(b) Thermocouple 10.

Figure 18.- Concluded.

Figure 19.- Typical curve of variation of length with capacitance for an ablation sensor.
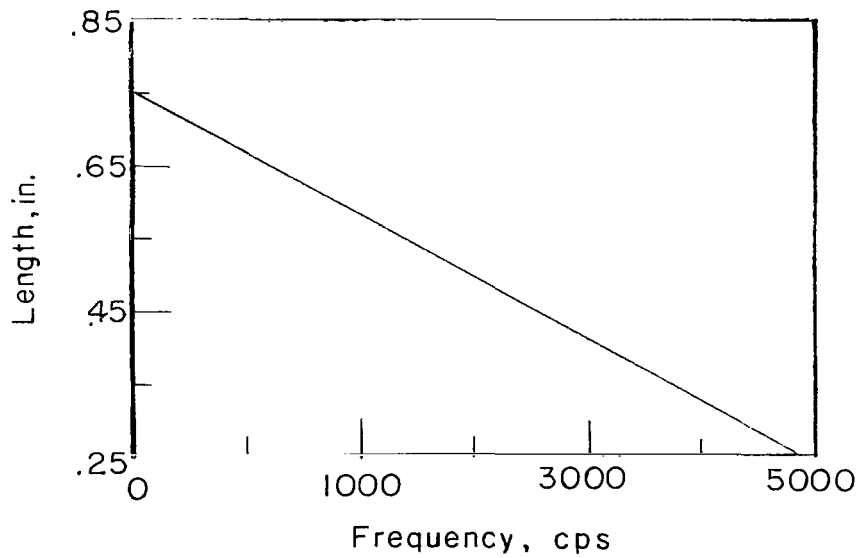

Figure 20.- Typical curve of variation of frequency with ablated length for an ablation sensor.

"The aeronautical and space activities of the United States shall be conducted so as to contribute . . . to the expansion of human knowledge of phenomena in the atmosphere and space. The Administration shall provide for the widest practicable and appropriate dissemination of information concerning its activities and the results thereof."

—NATIONAL AERONAUTICS AND SPACE ACT OF 1958

NASA SCIENTIFIC AND TECHNICAL PUBLICATIONS

TECHNICAL REPORTS: Scientific and technical information considered important, complete, and a lasting contribution to existing knowledge.

TECHNICAL NOTES: Information less broad in scope but nevertheless of importance as a contribution to existing knowledge.

TECHNICAL MEMORANDUMS: Information receiving limited distribution because of preliminary data, security classification, or other reasons.

CONTRACTOR REPORTS: Technical information generated in connection with a NASA contract or grant and released under NASA auspices.

TECHNICAL TRANSLATIONS: Information published in a foreign language considered to merit NASA distribution in English.

TECHNICAL REPRINTS: Information derived from NASA activities and initially published in the form of journal articles.

SPECIAL PUBLICATIONS: Information derived from or of value to NASA activities but not necessarily reporting the results of individual NASA-programmed scientific efforts. Publications include conference proceedings, monographs, data compilations, handbooks, sourcebooks, and special bibliographies.

Details on the availability of these publications may be obtained from:

SCIENTIFIC AND TECHNICAL INFORMATION DIVISION

NATIONAL AERONAUTICS AND SPACE ADMINISTRATION

Washington, D.C. 20546